Cellular and Molecular Neurobiology (2025) 45:10
https://doi.org/10.1007/s10571-024-01516-y

ORIGINAL RESEARCH

A Focal Traumatic Injury to the Neonatal Rodent Spinal Cord Causes an Immediate and Massive Spreading Depolarization Sustained by Chloride Ions, with Transient Network Dysfunction

Atiyeh Mohammadshirazi[1,2] · Graciela L. Mazzone[3,4] · Benjamín A. Zylberberg[3,4] · Giuliano Taccola[1,2]

Received: 27 August 2024 / Accepted: 13 November 2024

Abstract

In clinics, physical injuries to the spinal cord cause a temporary motor areflexia below lesion, known as spinal shock. This topic is still underexplored due to the lack of preclinical spinal cord injury (SCI) models that do not use anesthesia, which would affect spinal excitability. Our innovative design considered a custom-made micro impactor that provides localized and calibrated strikes to the ventral surface of the thoracic spinal cord of the entire CNS isolated from neonatal rats. Before and after injury, multiple ventral root (VR) recordings continuously traced respiratory rhythm, baseline spontaneous activities, and electrically induced reflex responses. As early as 200 ms after the lowering of the impactor, an immediate transient depolarization spread from the injury site to the whole spinal cord with distinct segmental velocities. Stronger strikes induced higher potentials causing, close by the site of injury, a transient drop in spinal cord oxygenation (SCO_2) and a massive cell death with a complete functional disconnection of input along the cord. Below the impact site, expiratory rhythm and spontaneous lumbar activity were suppressed. On lumbar VRs, reflex responses transiently halted but later recovered to control values, while electrically induced fictive locomotion remained perturbed. Moreover, low-ion modified Krebs solutions differently influenced impact-induced depolarizations, the magnitude of which amplified in low Cl^-. Overall, our novel ex vivo platform traces the immediate functional consequences of impacts to the spinal cord during development. This basic study provides insights on the SCI pathophysiology, unveiling an immediate chloride dysregulation.

Graphical Abstract

In a neonatal rodent preparation of ex vivo CNS, a physical trauma to the cord is followed by an immediate depolarization spreading both caudally and rostrally. A massive impact-induced depolarization temporarily abolishes spontaneous motor discharges and electrically induced reflex responses below the level of injury. Transient areflexia mimics the spinal shock reported in clinics after SCI.

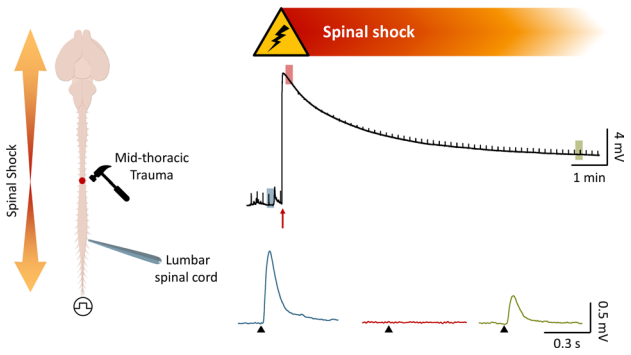

Keywords Spinal shock · Motor evoked potentials · Fictive locomotion · Isolated central nervous system · Spinal cord oxygenation · Neonatal SCI

Extended author information available on the last page of the article

Published online: 02 January 2025

Abbreviations

ANOVA	Analysis of variance
C	Cervical
CCF	Cross-correlation function
Ca^{2+}	Calcium ions
Cl^{-}	Chloride ions
CNS	Central nervous system
Ctrl	Control
CV	Coefficient of variation
DAPI	4′,6-Diamidino-2-phenylindole
DR	Dorsal root
DRG	Dorsal root ganglia
FL	Fictive locomotion
K^{+}	Potassium ions
l	Left
L	Lumbar
P	Postnatal
PO_2	Partial pressure of oxygen
r	Right
SCI	Spinal cord injury
SCO_2	Spinal cord oxygenation
SD	Spreading depression
Th	Threshold
T	Thoracic
VR	Ventral root

Introduction

A spinal cord injury (SCI) demonstrates that the mature central nervous system (CNS) of mammalians cannot regenerate nor repair itself after traumatic insults. Because of this vulnerability, an SCI often causes a permanent loss of sensory and motor control over the body parts innervated by spinal neurons located below the level of injury. Eventually, an SCI results in a life-long debilitating condition characterized by motor paralysis and a variegated spectrum of functional deficits and complications. To date, there is no cure against paralysis and current rehabilitation still focuses mainly on strengthening the able part of the body to compensate for the loss of volitional motor control over the rest. Support in daily tasks mainly occur through classical mobility aids, such as a wheelchair and crutches, but also using newly introduced technologies, such as exoskeletons (Gad et al. 2017) and advanced brain machine interfaces (Lorach et al. 2023), which however allow only minor functional benefits.

Nevertheless, some scattered and unpredictable spontaneous neurologic recoveries have been reported (Kirshblum et al. 2021) and, in less severe injuries, a substantial spontaneous regain of functions plateaued at 16 weeks after injury (Geisler et al. 2001). Spontaneous recoveries still challenge our understanding of the pathophysiological mechanisms of an SCI and of the residual potential of the cord to repair spinal circuits.

In particular, pediatric spinal injuries, which account for 1–10% of all SCIs (Carreon et al. 2004), show higher rates of spontaneous functional recovery compared to adults (Eleraky et al. 2000; Wang et al. 2004). Likewise, the study of traumatic injuries in the developing mammalian spinal tissue, also in comparison with adults (Clarke et al. 2009), is compelling to clarify the peculiar pathophysiological mechanisms of neonatal SCIs, in the hope to identify the reasons for the enhanced recoveries in children and possibly expand them to all people with SCI.

All preclinical models of SCI use adult mammals (Kjell and Olson 2016) under anesthesia. However, when administered near the time of injury, anesthetics affect the damage progression as, based upon the different drug adopted, they can exert a neuroprotective effect (Salzman et al. 1993; Davis and Grau 2023) or, on the contrary, exacerbate the hypoxic neuronal injury caused by transitory hypotension (Robba et al. 2017). In addition, up to date, only few reports described standardized and calibrated SCI models using immature spinal tissues isolated ex vivo (Taccola et al. 2010; Mladinic et al. 2013).

Another missing tile for the overall understanding of an SCI is the identification of the immediate events that take place during a physical injury to the spinal cord. In particular, it is still unknown how the primary mechanical insult to the spinal tissue contributes to trigger the subsequent cascade of pathological events known as secondary damage, which eventually determines the extent of tissue damage and hinders the chances of achieving a functional recovery (Carlson et al. 1998). Indeed, after injury, a temporary loss or depression of all, or most, spinal reflex activity takes place below the lesion. This phenomenon is called spinal shock, and the underlying mechanisms are not fully clarified (Ditunno et al. 2004). A spinal shock clinically persists for days or weeks, depending on which reflex is clinically being tested for reappearance. However, when duration is defined based on the initial recovery of any one reflex, then the spinal shock lasts no longer than 20–60 min (Ditunno et al. 2004). The lack of reflex activity has been mainly attributed both to the sudden disappearance of the predominantly facilitatory tonic influence exerted by descending supraspinal tracts, and to an increased presynaptic inhibition. In addition, depression of synaptic activities also depends on the hyperpolarization of spinal neurons due to an increased efflux of potassium from the damaged site that also blocks the axon conduction in white matter tracts (Eidelberg et al. 1975). In pediatric SCIs, reflexes recover sooner, likely because descending supraspinal tracts in children are not fully developed, thereby normal descending inhibition to spinal inhibitory pathways is less affected by an SCI compared to adults,

mitigating the depression of spinal networks during shock (Guttmann 1976).

Experimentally, the main features of a spinal shock parallel those of an early depolarization of the entire spinal cord following a trauma, also known as injury potential, which spreads rostrally and caudally from the site of impact. This early depolarization is sustained by a transient extracellular ionic disbalance (Goodman et al. 1985; Wang et al. 2015) and is similar to a cortical spreading depression (SD), which exhibits a marked, enduring reduction in the intrinsic electrical activity of neurons, eventually spreading from the original source out in all directions and involving increasingly distant parts of the cerebral cortex (Leao 1944, 1947). A cortical SD is triggered, among other causes (Gerasimova et al. 2021), by traumatic brain injuries (Hermann et al. 1999). In both amphibians and rodents, a compressive injury to the cord is followed both by SD-like waves characterized by a velocity of propagation of around 10–15 mm/min, and by a rapid and reversible increase in extracellular concentrations of K^+ ions (Streit et al. 1995; Gorji et al. 2004). Interestingly, electrically evoked potentials were transiently abolished during spinal SD waves, eventually returning to baseline values only after about 20 min. This phenomenon suggests that spinal SD might determine areflexia after spinal shock (Gorji et al. 2004). The same study also described how the SD evoked by an injury to the brain cortex reduced excitability of spinal neurons located in upper spinal segments, indicating that SD-like waves induced by an injury maintain a form of conduction among cortical and spinal structures (Gorji et al. 2004).

Obstacles to the comprehension of a spinal shock reside in some technical challenges that arise from the preclinical models currently available. Indeed, fully anesthetized animal models do not allow for recordings of the electrical activity of spinal neurons during a physical injury, due to both motion and electrical artifacts generated by standard experimental impactors, which interfere with the low amplitude of currents involved. As a consequence, the earliest injury potential has been recorded only after 4 min from the impact (Goodman et al. 1985). This temporal limitation adds to the effects of anesthetics that depress neuronal excitability and are used in preclinical models at the time of the physical trauma. A solution to avoid any technical artifacts, as well as any consequences of anesthetics, is the adoption of the neonatal preparation of the entire central nervous system ex vivo (CNS; Mohammadshirazi et al. 2023; Apicella and Taccola 2023), which does not require the administration of any drugs. In addition, the rodent spinal cord can be optimally damaged through a low-noise calibrated micro impactor recently designed in the laboratory.

Using this setting, we aim at monitoring the immediate electrophysiological changes in the network output at the moment of a physical insult to the cord, and how these variations respond to modified extracellular ion concentrations. Moreover, we seek to provide a histological assessment of neuronal damage at the injury site, and to explore the integrity of lumbar motor pools. Eventually, we will assess any spontaneous functional recoveries occurring in the neonatal spinal circuitry in the first two hours post injury.

Methods

Ex Vivo Preparation of the Isolated Entire CNS

All procedures were approved by the International School for Advanced Studies (SISSA) ethics committee and are in accordance with the guidelines of the National Institutes of Health (NIH) and the Italian Animal Welfare Act 24/3/2014 n. 26, implementing the European Union directive on animal experimentation (2010/63/EU). Every effort was made to minimize the number of animals used and to ensure their well-being. A total of 92 postnatal (P) Wistar rats (P0–P3) of random sexes were included in this study.

Experiments were performed on ex vivo preparations of the entire isolated central nervous system (CNS; Mohammadshirazi et al. 2023). Newborn rats were subjected to cryoanesthesia (Danneman and Mandrell 1997) for 8.24 ± 1.40 min. After disappearance of the paw pinch reflex, surgical procedures considered the quick removal of forehead at orbital line, ribs cage, internal stomach and forelimbs. The preparation was then transferred to a petri dish filled with oxygenated Krebs solution that contained (in mM): 113 NaCl, 4.5 KCl, 1 $MgCl_2 7H_2O$, 2 $CaCl_2$, 1 NaH_2PO_4, 25 $NaHCO_3$, and 30 glucose, gassed with 95% O_2—5% CO_2 (partial pressure of oxygen, $PO_2 = 533.65 \pm 44.05$ Torr), pH 7.4, 299.62 ± 3.2 mOsm/kg. Under microscopic guidance, craniotomy and ventral vertebrectomy were performed keeping the dorsal vertebral processes and dorsal root ganglia (DRG) intact. The isolation of the CNS required an overall time of 22.55 ± 2.92 min. Afterwards, the entire CNS preparation was maintained in oxygenated Krebs solution at room temperature for 15 min and then mounted in the recording chamber (total volume = 4.7 mL, flow rate = 7 mL/min, controlled temperature = 25–27 °C, TC-324C Warner Instruments, USA). For stable electrophysiological recordings, the preparation was fixed ventral side up with insect pins passing through dorsal vertebrae. For selective root recordings, ventral roots (VRs) and dorsal roots (DRs) were detached from DRG.

Extracellular Recordings

DC-coupled recordings were obtained from both VRs and DRs using monopolar suction electrodes realized by pulling tight-fitting glass pipettes (1.5 mm outer diameter,

0.225 mm wall thickness; Hilgenberg, Germany). The tip of each pipette was filled with Krebs physiological solution and, using micromanipulators, was positioned on targeted VRs and DRs. Then, a gentle negative pressure was applied to draw the root extremity inside the pipette. Afterwards, the pipette was moved close to the origin of the targeted VR and, through further pressure, the entire root was suctioned into the glass pipette. Electrodes were connected to a differential amplifier (DP-304, Warner Instruments, Hamden, CT, USA; high-pass filter = 0.1 Hz, low-pass filter = 10 kHz, gain X 1000). Analog signals were filtered through a noise eliminator (D400, Digitimer Ltd, UK), then digitized (Digidata 1440, Molecular Devices Corporation, Downingtown, PA, USA; digital Bessel low-pass filter at 10 Hz; sampling rate = 5 kHz) and visualized real-time with the software Clampex 10.7 (Molecular Devices Corporation, Downingtown, PA, USA).

Electrical Stimulation

Trains of rectangular electrical pulses (pulse duration = 0.1 ms, frequency = 0.1 Hz) were supplied to sacrocaudal afferents through a programmable stimulator (STG4002, Multichannel System, Reutlingen, Germany) using bipolar glass suction electrodes connected two close silver wires (500–300 µm). Stimulus intensity (40–160 µA) was attributed as times to threshold (Th), where Th is the lowest intensity required to elicit a small deflection of VRrL5 baseline. To generate epochs of fictive locomotor patterns (Kiehn 2006), 160 rectangular pulses (duration = 0.1 ms, intensity = 37.5–150 µA, 1–5 × Th) were supplied at 2 Hz to sacrocaudal afferents for a total length of 80 s. Recordings were acquired in the same preparation from right (r) and left (l) VRL2 (for bilateral flexor commands) and VRrL5 (for extensor output).

Spinal Cord Injury

A calibrated physical injury to the thoracic (T) cord was provided using a custom-made micro-impactor device specifically designed and shielded to allow simultaneous electrophysiological recordings from the neonatal CNS ex vivo. The device is currently being patented by SISSA and is available upon request (https://www.valorisation.sissa.it/device-mechanically-stimulating-biological-material-and-its-procedure). Using a manipulator, the impactor tip (diameter = 2 mm) was precisely positioned on the ventral surface of the spinal cord (T10, diameter around 1–1.5 mm) that maintains a distance of 3–4 mm from the floor of the recording chamber due to the dorsal spine below. The micro-impactor was controlled through a dedicated software that allows to precisely set impact parameters (displacement, speed, acceleration, deceleration, and pause time). Time of impact to the cord was calibrated by a digital pulse provided by the impactor at the beginning of its actual movement. To assess the strongest severity of contusion to apply without lacerating the spinal tissue, serial vertical displacements and velocities of the impactor rod were considered (625 µm at 2 mm/s, 1250 µm at 2.8 mm/s, 1875 µm at 3.4 mm/s and 2656 µm at 4 mm/s), while keeping acceleration and deceleration constant (6.1 ± 0.05 mm/s^2). After the impact, the tip of the impactor was promptly returned to its original position at the same speed, acceleration, and deceleration. In five preparations, the four different strengths of compression were serially applied to the spinal cord at T10 (SI. Fig. 1). In our experiments, the maximum severity of compression without completely transecting the neonatal spinal cord was obtained with the impactor tip descending into the cord by 2656 µm from the spinal surface, at an average speed of 4 mm/s, maintaining an acceleration and deceleration of 6.1 ± 0.05 mm/s^2.

Modified Krebs Solutions

Three modified Krebs solutions were prepared. The low chloride solution (in mM) was composed of 56.5 NaCl, 56.5 sodium isethionate, 4.5 KCl, 1 $MgCl_2 7H_2O$, 2 $CaCl_2$, 1 NaH_2PO_4, 25 $NaHCO_3$, and 30 glucose (297.62 ± 3.8 mOsm/kg). The low calcium solution (in mM) contained: 113 NaCl, 4.5 KCl, 1 $MgCl_2 7H_2O$, 1 $CaCl_2$, 1 NaH_2PO_4, 25 $NaHCO_3$, and 30 glucose. The low potassium solution (in mM) was prepared with 113 NaCl, 2.25 KCl, 1 $MgCl_2 7H_2O$, 2 $CaCl_2$, 1 NaH_2PO_4, 25 $NaHCO_3$, and 30 glucose. The three modified Krebs solutions were gassed with 95% O_2—5% CO_2 and their osmolarity was adjusted by adding sucrose to the osmolarity of control Krebs solution. To assess the different impact of modified Krebs solutions on spinal reflexes, analysis was performed on five responses randomly chosen in control, and five in the last 2 min of low-ion perfusions.

Assessment of Spinal Cord Oxygenation

PO_2 measurements in the spinal cord were conducted using a fiber-optic microsensor with a 50 µm tip diameter (Optode, OxyMicro System, World Precision Instruments, FL, USA). The microsensor was implanted at 100 µm deep into the cord in the ventral funiculus between L1 and L2 segments. Measurements were taken at the sampling rate of one per second and were directly acquired using OxyMicro v7.0.0 software (OxyMicro System, World Precision Instruments, FL, USA). Temperature during all PO_2 measurements was maintained within the range of 25–27 °C.

To ascertain whether high K^+ perfusions affect measurements of the microsensor probe, test experiments considered positioning the tip of the microsensor in the recording chamber void of any preparation. PO_2 values remained

unchanged in standard Krebs solution (610.29 ± 7.63) and during 10 mM K^+ applications (613 ± 8.53) indicating that tissue oxygen assessments did not change during perfusion with potassium ions (SI. Fig. 2B).

Tissue Section Immunostaining and Cell Counting

After electrophysiological experiments, spinal cords were fixed overnight in 4% paraformaldehyde at 4 °C and then tissue was cryopreserved with 30% sucrose in phosphate buffered saline (PBS), following our standard procedures (Taccola et al. 2008, 2010). Spinal cords were cut in 20 µm (coronal or longitudinal) tissue sections using a sliding cryostat microtome. To detect neurons and motoneurons, tissue sections were incubated at 4 °C with a blocking solution for 1 h and then overnight with mouse monoclonal antibodies for anti-NeuN (1:200; catalog # ABN78, Merck Millipore, Milan, Italy), SMI 32 (1: 200; catalog # SMI-32P, Covance, Berkeley, CA) in 5% fetal calf serum (FCS), 5% bovine serum albumin (BSA), and 0.3% Triton X-100 in PBS. After three washes in PBS, floating sections were incubated for 2 h at room temperature with the goat anti-mouse Alexa 488-labeled secondary antibody (1:500, Invitrogen). To visualize cell nuclei, tissue sections were incubated in 1 µg/mL solution of 4′,6-diamidino-2-phenylindole (DAPI). Sections were washed three times in PBS for 5 min and mounted using Vectashield® medium (Vector Laboratories, Burlingame, CA) and coverslips. SMI 32 positive cells were assessed in a complete set of z-stack images, typically at a depth of 4-µm, using confocal series acquired by Nis-Eclipse microscope (NIKON, Amsterdam, Netherlands, objective Plan Fluor × 20 DIC M N2, × 20 magnification, 0.5 numerical aperture, pinhole size 60). The number of SMI 32 positive cells was determined by Volocity™ software (version7, Quorum Technologies Inc., Puslinch, CA) and normalized to the total number of DAPI labeled nuclei in the region of interest (ROI). The number of NeuN positive cells was obtained by counting images obtained using a Nis-Eclipse microscope (NIKON, Amsterdam, Netherlands, objective Plan Apo λ, × 20 magnification, 0.75 numerical aperture, wide-field fluorescence). The NeuN counting for the injury site was performed considering segments from T9 to T11 and centered at T10, while the range spanned from T11 to L1 spinal roots for the caudal region and from T9 to T6 spinal roots for rostral spinal segments. The number of NeuN positive cells was counted with Image J software (version 1.54J, Wayne Rasband, National Institutes of Health, Bethesda, MD, USA, https://imagej.nih.gov/ij/index.html) and normalized to the total number of DAPI labeled nuclei in the ROI.

Data Analysis

Data analysis was performed using Clampfit 10.7 software (Molecular Devices Corporation, PA, USA). Spontaneous rhythmic motor discharges recorded from cervical VRs, with a period of 24.27 ± 16.13 s, were attributed to respiratory bursts that were also derived synchronous among bilateral lumbar VRs (Nicholls et al. 1990; Iizuka 1999; Mohammadshirazi et al. 2023; Apicella and Taccola 2023). The coefficient of variation (CV), an indicator of response consistency, was determined by the ratio between standard deviation and mean value (Taccola et al. 2020). To calculate conduction velocity, the latency of each response was divided by the distance between the center of the impacted area and the recording sites, as precisely measured using a microcalibrated dial caliper (sensitivity = 20 µm). The correlation coefficient function (CCF) was used to measure phase coupling between pairs of VRs using Clampfit 10.7 software. A CCF value ≥ 0.5 indicates synchronous rhythmic signals from two VRs, while a CCF value ≤ -0.5 indicates alternating signals (Taccola and Nistri 2005; Dose et al. 2016).

Statistical Analysis

Statistical analysis was performed with GraphPad InStat 3.10 (Inc., San Diego, California, USA). In the Results section, the number of animals is denoted as "*n*", and data is presented as mean ± standard deviation (SD) values. Before conducting comparisons among groups, a normality test was performed to select the appropriate parametric or non-parametric tests. Parametric data were analyzed with paired student *t*-test, one-way analysis of variance (ANOVA) or repeated measure analysis, while non-parametric data were analyzed using Kruskal–Wallis, Mann–Whitney, Friedman, or Wilcoxon matched-pairs signed-ranks tests. Multiple comparisons ANOVA was followed by Tukey–Kramer, Dunn's or Dunnett multiple comparisons tests. Differences were considered statistically significant when p value ≤ 0.05.

Data distributions were visualized using box-and-whisker plots generated in Excel (Microsoft, WA, US). The box-and-whisker plots display the interquartile range (IQR), with the lower and upper bounds of the box representing the first (Q1) and third quartiles (Q3), respectively. The line inside the box shows the inclusive median, and the mean value is marked by a cross. Whiskers extend to the most extreme data points that are within 1.5 times the IQR from the box edges, while any outliers beyond this range are individually plotted as dots.

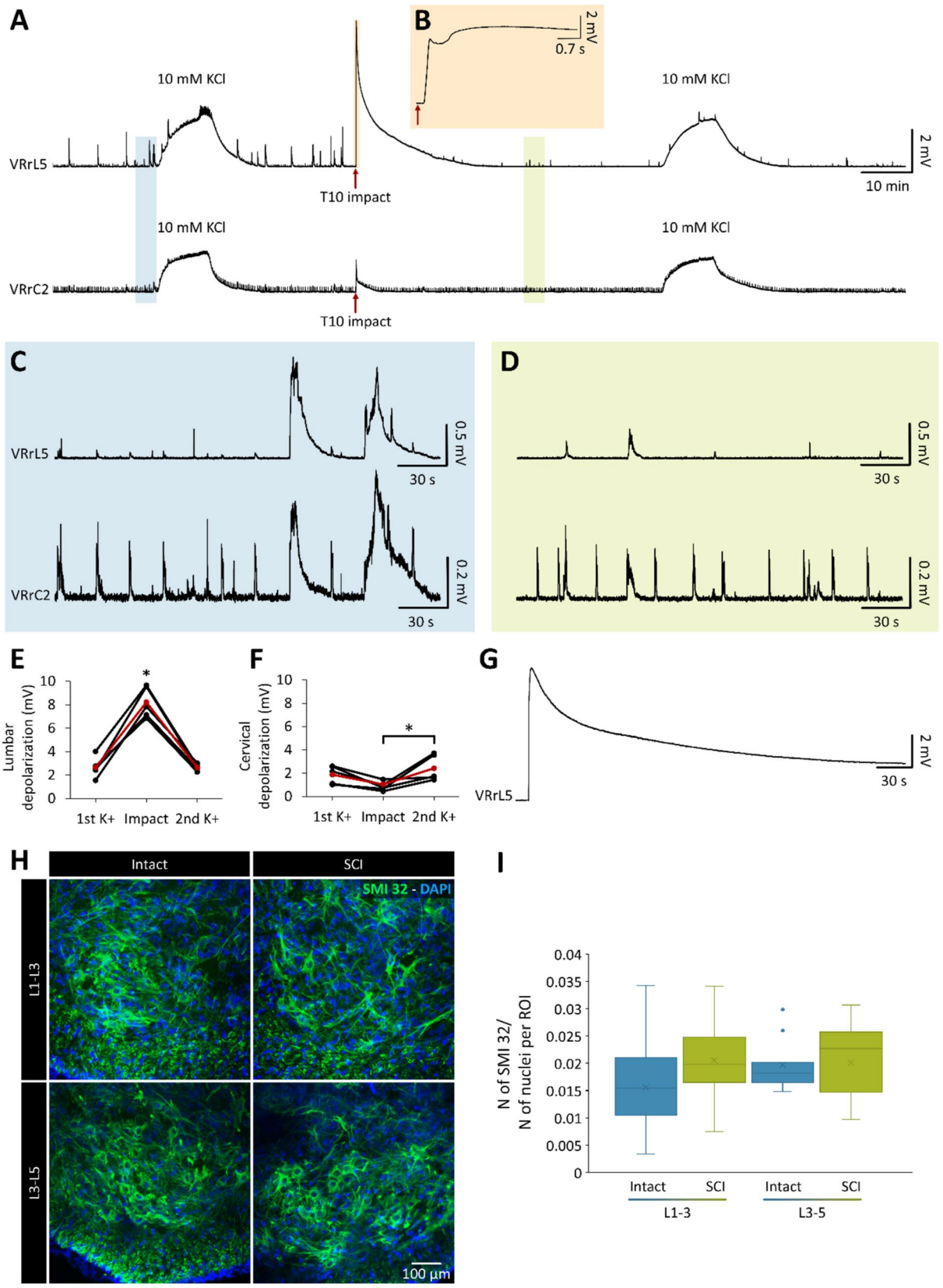
A
10 mM KCl
10 mM KCl
VRrL5
T10 impact
2 mV
10 min
10 mM KCl
10 mM KCl
VRrC2
T10 impact
B
2 mV
0.7 s
C
VRrL5
0.5 mV
30 s
VRrC2
0.2 mV
30 s
D
0.5 mV
30 s
0.2 mV
30 s
E
Lumbar depolarization (mV)
1st K+ Impact 2nd K+
F
Cervical depolarization (mV)
1st K+ Impact 2nd K+
G
VRrL5
2 mV
30 s
H
Intact
SCI
SMI 32 - DAPI
L1-L3
L3-L5
100 µm
I
N of SMI 32/ N of nuclei per ROI
Intact SCI Intact SCI
L1-3
L3-5

◂**Fig. 1** A transient depolarization immediately follows a physical injury to the spinal cord. **A** Long continuous recordings from VRrL5 and VRrC2, while the cord is being impacted at T10 (red arrows). An injury-induced potential occurs after 194.4 ms from the onset of the impact on VRrL5, and after 225.2 ms on VRrC2. On VRrL5, a depolarization peak of 6.86 mV is reached after 2.66 s, followed by a depolarizing plateau lasting 3.52 s and spontaneously recovering to baseline in less than 15 min. VRrC2 generated a smaller depolarization peak (1.47 mV). Before and after the impact, 10 mM KCl were perfused for ten minutes to compare the recruitment of motor pools. Before the impact, KCl generated depolarizations that were smaller on VRrL5 (40.34%) and greater on VRrC2 (177.9%), compared to the ones induced by the following impact. A second exposure to 10 mM KCl after injury produced on both VRs the same depolarizations as the pre-impact application. **B** Magnification highlights the depolarization at VRrL5 in the first five seconds after impact (red arrows). **C** and **D** Faster time scales of VR traces in **A**, corresponding to the shaded blue and green fields that are recorded before and after the impact, respectively. After the impact, spontaneous sporadic bursting from VRs is largely reduced by the trauma. **E** Pooled data from five experiments, displays an amplitude of impact-induced depolarization recorded from VRrL5 that significantly exceeds the depolarization-induced by 10 mM KCl before and after the impact (*$P < 0.001$, repeated measures ANOVA followed by Dunnett all pairwise multiple comparisons test, $n = 5$). Mean values are indicated by the red dots and line. **F** In cervical motor pools, depolarization after injury is notably smaller than after a second application of potassium (*$P = 0.046$, repeated measures ANOVA followed by Dunnett all pairwise multiple comparisons test, $n = 5$). Mean values are indicated by the red dots and line. **G** Superimposed depolarizations from VRrL5 in five experiments. **H** SMI 32 labeling of samples collected 90 min after the impact display a comparable number of motoneurons in L1 to L3, and in L3 to L5 segments of both, intact and SCI experiments. **I** Box-and-whisker plots for the number of SMI 32 positive cells normalized to the total number of nuclei in the region of interest (ROI) show no statistical changes caudal to the injury site (L1–L3 and L3–L5, $P = 0.360$, ANOVA followed by Tukey–Kramer all pairwise multiple comparisons test, $n = 4$ intact, $n = 4$ SCI)

Results

A Physical Injury to the Cord Elicits an Immediate Depolarizing Potential

To investigate the immediate events following a contusive spinal cord injury, a custom-made impactor was employed to induce a physical injury at thoracic spinal cord level of an ex vivo preparation of entire CNS (Mohammadshirazi et al. 2023). The careful design of the impactor included a proper shielding to minimize any electrical interference during operation, to allow simultaneous electrophysiological recordings during the impact. In an exemplar experiment, a brief and intense impact (duration = 1.30 s, displacement = 2656 µm) on the ventral cord (T10) led to a massive depolarization, recorded rostral and caudal to the compression site from cervical and lumbar VRs, respectively (Fig. 1A, B). The profile of the average injury-induced potential from VRrL5 reveals a peak of 8.21 ± 1.32 mV and a latency of 178.41 ± 15.17 ms after the impact, recovering to 81.11 ± 12.56% 6 min later ($n = 5$; Fig. 1G). A milder impact (displacement = 625 µm) applied to another group of five preparations elicited a smaller injury-induced potential from VRrL5 (SI. Fig. 1A), with a peak of 0.76 ± 0.38 mV (SI. Fig. 1B) and a latency of 180.84 ± 24.61 ms (SI. Fig. 1C), which recovered to baseline just 2 min later.

Sporadic episodes of spontaneous motor discharges appear synchronous among all motor pools of the isolated neonatal spinal cord as a result of the motor activity reverberating through a diffuse propriospinal network (Cazalets 2005). This activity was largely reduced on both VRrL5 and VRrC2, following an impact at T10 (Fig. 1C, D), as observed in 20 out of 24 preparations.

Each spinal segment owns a distinct number of motoneurons (Sadeghinezhad and Nyengaard 2021) that varies the absolute magnitude of each segmental motor pool recruitment. In addition, the amplitude of extracellular signals depends on the impedance of glass electrodes, which is mainly affected by the seal of the target spinal root. To quantify the peak of injury-induced depolarization in relation to the depolarization produced by the direct recruitment of motoneurons in each spinal segment and across different preparations, 10 mM potassium was applied to the bath for 10 min before the impact to the same exemplar preparation (Fig. 1A). A second exposure to 10 mM KCl was applied to ascertain the absence of any functional alterations of motor pools after the impact (Fig. 1A). Pooled data from five preparations showed that the peak of average injury-induced depolarizations from VRrL5 was significantly higher than the depolarizations elicited by 10 mM KCl ($P < 0.001$, repeated measures ANOVA followed by Dunnett all pairwise multiple comparisons test, $n = 5$; Fig. 1E). Conversely, in the same group of preparations, the average injury-induced depolarization from VRrC2 was lower than the one elicited at lumbar levels ($P < 0.001$), and significantly lower than the depolarization determined by a second application of 10 mM KCl (Fig. 1F; $P = 0.046$, repeated measures ANOVA followed by Dunnett all pairwise multiple comparisons test, $n = 5$). Notably, at both L5 and C2 levels, potentials elicited by rising KCl concentrations were comparable before and after the impact (Fig. 1E, F). This confirms that an injury targeted to the low thoracic cord (T10) does not reduce the overall availability of motoneurons located in motor pools far from the injury site, which remain equally functional once directly activated by KCl.

Furthermore, distinct lumbar segments of intact and injured spinal cords were treated with a selective marker for motoneurons in the ventral horns (SMI 32 antibody). Histological processing visualized a similar SMI 32 staining in the ventral cord of the intact and injured preparations, for both L1-L3 and L3-L5 segments (Fig. 1H). Mean data from 49 tissue sections from a total of eight animals (four intact and four injured spinal cords) confirmed no significant difference in the ratio of SMI 32 positive cells

(Fig. 1I; $P = 0.360$, ANOVA followed by Tukey–Kramer all pairwise multiple comparison test), hence excluding the acute death of any lumbar motoneurons after the low thoracic injury and related spread depolarization.

Collectively, a physical insult to the mid-thoracic spinal cord triggers a transient and massive depolarization spreading along the entire spinal cord, suppressing the spontaneous motor activity that is derived synchronous among all neonatal VRs, yet without any cellular loss of lumbar motor pools.

Injury Potentials Originate from Actual Neuronal Depolarizations

To confirm that the observed sudden increment in DC levels is indeed a genuine potential rather than an artifact, we performed supplementary tests. Firstly, in five experiments, repeated impacts of increasing strength on the same preparations (SI. Fig. 1) demonstrated that stronger impacts (625 µm, 1250 µm, 1875 µm) produce higher potentials. However, an additional increase in the intensity of the trauma (2656 µm) failed to further increase the amplitude of injury potentials, likely due to the repetitive damage to the cord at the same site of impact (SI. Fig. 1). Overall, any electrical interference produced by the engine of the device remained equal whenever the device was activated, regardless the extent of rod displacement. Conversely, the increasing potentials obtained in the present study in response to greater impact strengths prove the direct relationship between the severity of impact and the extent of VR depolarization.

Another test considered the device acting solely on the bath, close to the preparation, but without touching the cord (SI. Fig. 3A, B), revealing the absence of any potentials generated by the impactor engine. Furthermore, in four experiments, multiple impacts of equal severity (displacement = 2656 µm) were serially applied to the same site (T10) for five times, with a lag of less than 10 s between any two consecutive impacts. As a result, peaks of injury-induced potentials remained stable, excluding any summation of artifacts (SI. Fig. 3C). On the other hand, when the impact was delivered at the top of a large depolarization (16.46 mV) that was evoked by 50 mM KCl, no injury-evoked depolarization appeared (SI. Fig. 3D). Finally, in another preparation, no baseline deflections were recorded from VRrL5 when the impact was inflicted to the T10 segment of a spinal tissue inactivated by both high temperature (100 °C) and long-lasting (1 h) oxygen deprivation (SI. Fig. 2C), proving the biological origin of depolarization after injury.

Collectively, these tests revealed the absence of any significant baseline drift produced either by the engine itself or by the sudden movement of the tip in the recording bath.

Injury Potentials Propagate Rostrally and Caudally from the Site of Impact in Ventro-Dorsal Directions

To better investigate the propagation of injury-induced depolarization along the entire spinal cord, we collected data from numerous VRs, out of a dataset of 44 preparations injured at the ventral aspect of T10 with the strongest impact (2656 µm tip displacement, Fig. 2A). Injury potentials of different amplitude were recorded from distinct spinal segments, with the highest peaks from VRL1 and L2 being significantly larger than those derived at the extremities (Fig. 2B, see Table 1 for statistical details). Injury potentials progressively slowed down the farther they were recorded from the impact site, with the lowest latency recorded at VRL1 (Fig. 2C, see Table 2 for statistical details). Resulting velocity of the rostro-caudal conduction of injury-induced depolarizations from the site of impact to VRL1 (4.44 mm far from impact) was 0.03 ± 0.01 m/s, equal to the caudo-rostral conduction from the site of impact to VRT5 (4.83 mm far from impact, $P = 0.451$, Mann–Whitney test, $n = 3$ for T5 and $n = 18$ for L1).

To gain insights on the dorsal–ventral propagation of injury-induced depolarization, we simultaneously derived from both VRrL1 and DRrL1 while impacting the ventral side of the cord at T10. Data pooled from many experiments (Fig. 2D) indicates that the impact leads to injury potentials that propagate also to the dorsal part of the cord, although they appear smaller (Fig. 2E; $P = 0.041$, paired t-test, $n = 5$) and spread more slowly (Fig. 2F; $P = 0.015$, paired t-test, $n = 4$) than ventrally elicited potentials.

Present data indicates that a physical injury to the spinal cord elicits a strong wave of depolarization that departs from the site of injury and invests the entire spinal cord with the same velocity, affecting also dorsal segments. This observation provides the rationale for ascertaining the functionality of spinal networks above and below the site of injury.

An Impact Generates Potentials that Equally Propagate to Both Sides of the Cord, and Functionally Disconnects the Lumbar Cord from Descending Respiratory Input

To confirm the symmetrical propagation of injury-induced depolarizations along both sides of the cord, simultaneous VR recordings were obtained from both left and right VRs at L1, in response to a physical injury at T10. In a sample experiment, continuous recordings were acquired from VRlL1, VRrL1, and VRrC2 (Fig. 3A). Average data from four experiments indicated an equal extent of impact-induced depolarizations on both sides of the L1 spinal segment (Fig. 3B, $P > 0.999$, Wilcoxon matched-pairs signed-ranks test, $n = 4$).

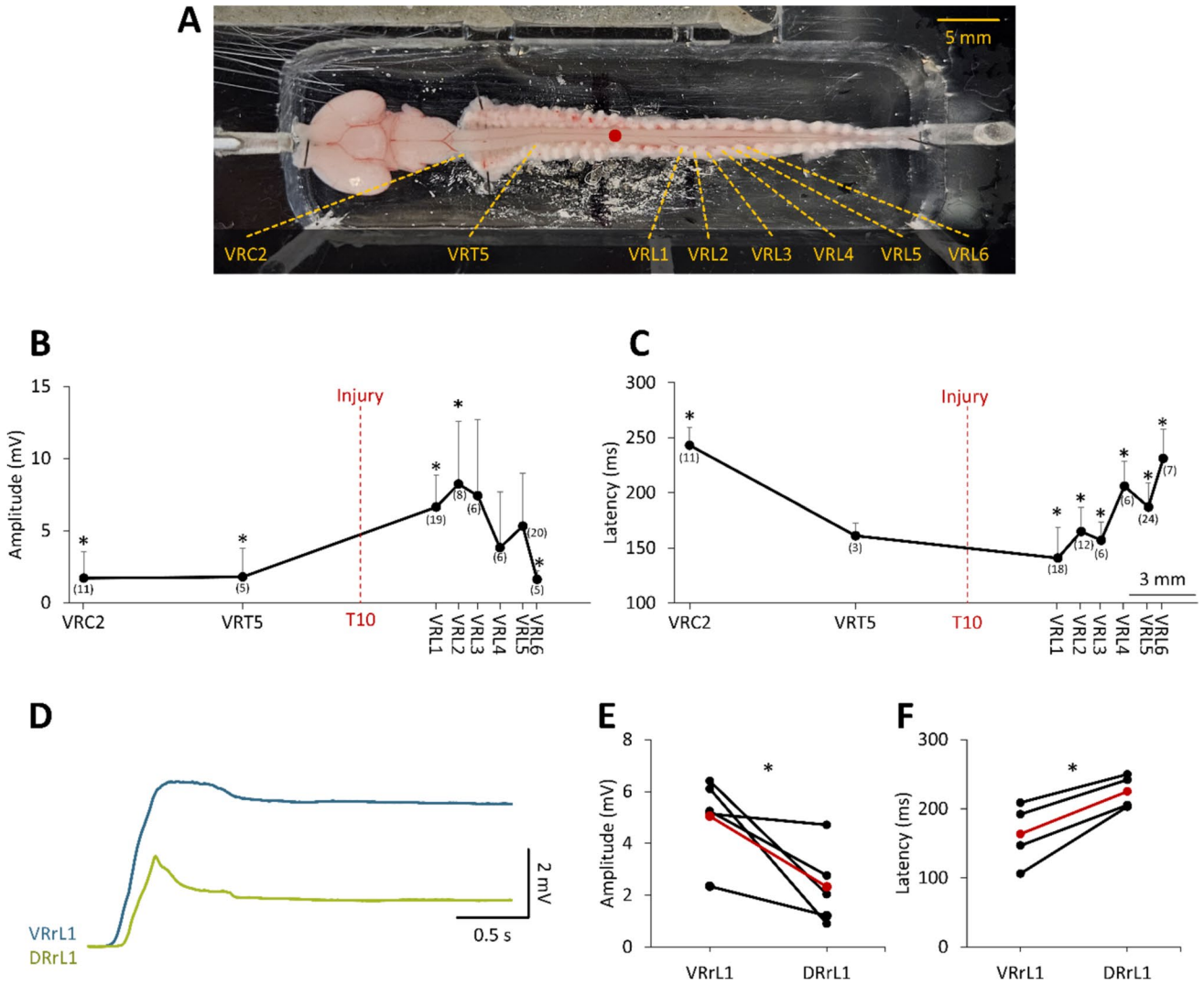

Fig. 2 Impact-induced depolarization spreads from the injury site to the whole spinal cord. **A** A ventral view of the CNS preparation with dorsal vertebrae attached. VRs recordings are taken from the VRs indicated by dotted yellow lines, while the injury site at the T10 segment is highlighted by a red dot. **B** Mean amplitudes of injury potentials from several VRs. Red dotted line indicates the level of injury (T10). Number of experiments for each VR is indicated in brackets. Statistically significant amplitudes are indicated by *, as described in Table 1. **C** Mean latencies of injury potentials from several VRs. Red dotted line indicates the level of injury (T10). Number of experiments for each VR is indicated in brackets. Statistically significant amplitudes are indicated by *, as described in Table 2. **D** Superimposed mean traces from simultaneous recordings of injury potentials from both, DR (green trace) and VR (blue trace), at L1 ($n=4$). **E** and **F** Injury potentials from DRrL1 are significantly smaller (**E**; $*P=0.041$, paired t-test, $n=5$) and slower (**F**; $*P=0.015$, paired t-test, $n=4$) than recorded from VRrL1. Red dots and line show average values

To monitor the respiration-related activity that originates by neuronal networks located in the brainstem (Del Negro et al. 2018), spontaneous rhythmic bursts were recorded from cervical VRs of the isolated CNS (Nicholls et al. 1990; Iizuka 1999; Mohammadshirazi et al. 2023; Apicella and Taccola 2023). To assess any early and transient alteration of the respiratory rhythm during the impact, 20 respiratory bursts from cervical VRs were analyzed right before and soon after the injury. In 4 out of 7 preparations, the first respiratory event after the impact was delayed, showing an early perturbation of the neuronal networks in the brainstem generating the respiratory rhythm (SI. Fig. 4). Albeit not consistent among all preparations, this effect was observed in the majority of experiments (57%), regardless of the magnitude of injury potentials from cervical VRs and the age of animals (SI. Fig. 4). Noteworthy, when assessed 30 min after injury, respiratory bursting recorded from upper cervical VRs, was not affected by the thoracic impact to the cord (Fig. 3C). In seven preparations, respiration frequency from VRC2 was $84.28 \pm 20.29\%$ of pre-impact control (0.05 ± 0.03 Hz from 20 min pre-injury, 0.05 ± 0.02 Hz from 20 min post-injury, $P=0.709$, paired t-test) with unaffected burst amplitude (0.29 ± 0.18 mV before

Table 1 Amplitude values of impact-induced depolarizations from different VRs

Amplitude								
Vs	VRC2	VRT5	VRL1	VRL2	VRL3	VRL4	VRL5	VRL6
VRC2		ns	$P<0.01$	$P<0.01$	ns	ns	ns	ns
VRT5	ns		ns	$P<0.05$	ns	ns	ns	ns
VRL1	$P<0.01$	ns		ns	ns	ns	ns	$P<0.05$
VRL2	$P<0.01$	$P<0.05$	ns		ns	ns	ns	$P<0.05$
VRL3	ns	ns	ns	ns		ns	ns	ns
VRL4	ns	ns	ns	ns	ns		ns	ns
VRL5	ns	ns	ns	ns	ns	ns		ns
VRL6	ns	ns	$P<0.05$	$P<0.05$	ns	ns	ns	
Average	1.72	1.79	6.64	8.23	7.42	3.83	5.33	1.6
SD	1.84	1.99	2.20	4.37	5.28	3.85	3.67	0.59
n	11	5	19	8	6	6	20	6

P values correspond to Kruskal–Wallis test followed by Dunn's all pairwise multiple comparisons test

Table 2 Latency values of impact-induced depolarizations from different VRs

Latency								
Vs	VRC2	VRT5	VRL1	VRL2	VRL3	VRL4	VRL5	VRL6
VRC2		ns	$P<0.001$	$P<0.001$	$P<0.001$	ns	$P<0.05$	ns
VRT5	ns		ns	ns	ns	ns	ns	ns
VRL1	$P<0.001$	ns		ns	ns	$P<0.01$	$P<0.01$	$P<0.001$
VRL2	$P<0.001$	ns	ns		ns	ns	ns	$P<0.05$
VRL3	$P<0.001$	ns	ns	ns		ns	ns	$P<0.05$
VRL4	ns	ns	$P<0.01$	ns	ns		ns	ns
VRL5	$P<0.05$	ns	$P<0.01$	ns	ns	ns		ns
VRL6	ns	ns	$P<0.001$	$P<0.05$	$P<0.05$	ns	ns	
Average	243.13	161.2	140.81	165.03	157.1	205.97	187.19	231.31
SD	16.36	11.79	28	22.14	16.7	22.84	21.68	26.62
n	11	3	18	12	6	6	24	7

P values correspond to Kruskal–Wallis test followed by Dunn's all pairwise multiple comparisons test

impact, 0.26 ± 0.21 mV after impact; $P = 0.195$, paired *t* test). Moreover, the respiratory rhythm can also be recorded from lumbar VRs, which drive the recruitment of chest muscles to assist the expiratory phase (Janczewski et al. 2002; Taccola et al. 2007; Giraudin et al. 2008). In seven experiments, the lumbar respiratory motor activity is abolished after trauma (Fig. 3 C).

In summary, the equal magnitude of bilateral injury potentials propagating to lumbar VRs confirms the midline location of the impact. Moreover, the disappearance of respiratory bursts below the site of injury indicates that lumbar motor pools are completely disconnected from supraspinal respiratory centers.

Impact Causes Extensive Neuronal Loss at the Contusion Site and Functionally Disconnects Ascending Afferent Input

Disappearance of respiratory episodes from the lumbar cord indicates that descending respiratory input from the brainstem are blocked at the level of impact. To investigate whether also the conduction of ascending input is blocked by the impact, we recorded ascending input evoked by continuous electric stimulations (intensity = 100 µA, pulse duration = 0.1 ms, frequency = 0.1 Hz) of sacrocaudal afferents (Etlin et al. 2010). Simultaneous recordings were taken above and below the level of impact. In a sample experiment,

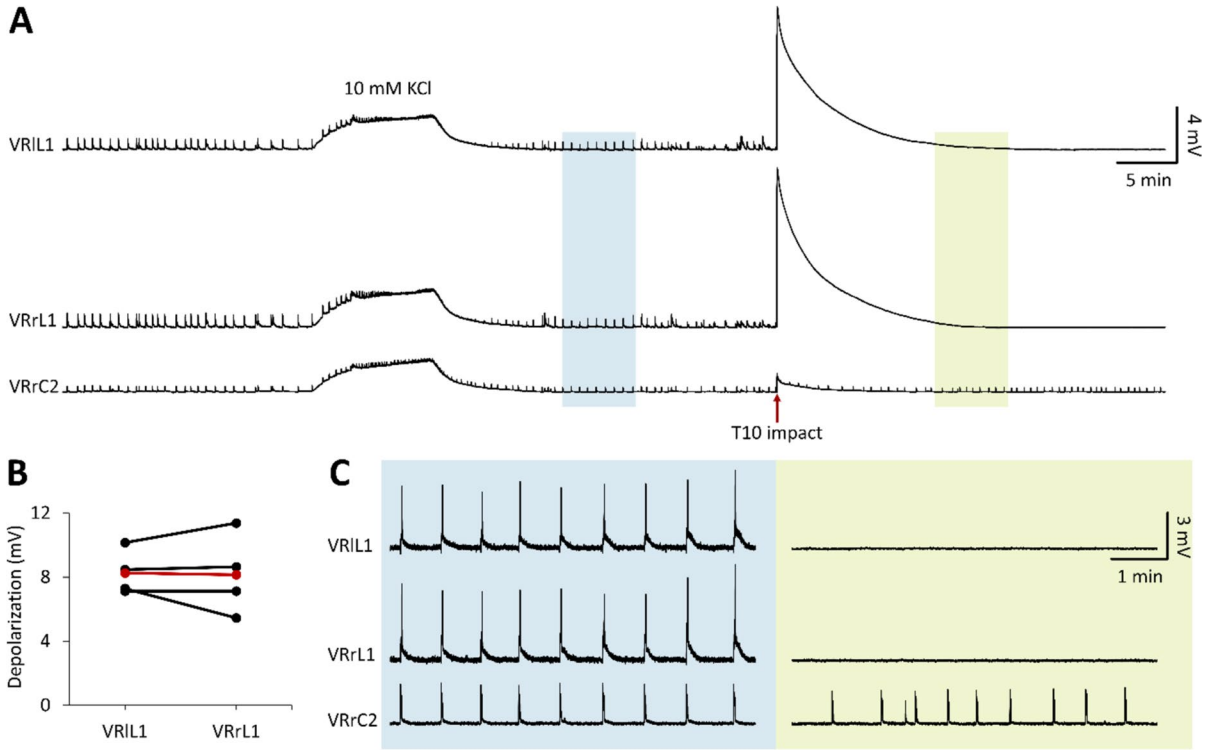

Fig. 3 Impact evokes equal bilateral injury potentials and disconnects lumbar motor pools from descending respiratory input. **A** Continuous and simultaneous recordings from VRrL1, VRlL1, and VRrC2 showing the exposure to 10 mM potassium (10 min) and to the following impact at T10. After the impact, VR injury-induced potentials peaked at 10.15 mV and 11.38 mV for left and right VRs, respectively. **B** The plot visualizes the equal amplitude of injury-induced depolarizations recorded from left and right L1 VRs ($P > 0.999$, Wilcoxon matched-pairs signed-ranks test, $n = 4$). Red dots and red line correspond to average values. **C** Magnifications correspond to the pale regions of continuous traces in **A**, and highlight rhythmic respiratory bursts in control (blue panel, 0.02 ± 0.01 Hz) and 21.8 min after the impact (green panel, 0.02 ± 0.01 Hz). Fictive respiration originating from brainstem structures is maintained at VRrC2 but disappeared from lumbar VRs due to the functional interruption of descending input beyond the site of impact

single reflex responses in control were recorded from VRrL5 and VRrC2, respectively (blue traces in Fig. 4A). At the peak of injury-induced depolarization, both responses vanished (Fig. 4A). After 38 s from the impact, reflex responses from VRrL5 reappeared and eventually stabilized after 8 min, albeit reduced in amplitude to 41% of pre-impact control. Contrariwise, cervical responses were completely abolished (green traces in Fig. 4A). The disappearance of cervical reflexes after the impact was replicated in nine out of nine preparations.

The suppression of both, respiratory lumbar episodes and cervical reflexes evoked by sacrocaudal stimulation, suggests a functional impairment of input conduction along the cord due to the impact. To visualize neuronal cell death caused by the impact, staining for neurons was performed on sagittal sections of the entire spinal cord. The ventral spinal cord at the site of impact (dotted yellow rectangle) showed negligible neuronal labeling for NeuN due to an extensive cell loss (Fig. 4B). In another example, magnifications of sagittal tissue sections from serial close spinal segments confirmed a lower number of NeuN positive cells at the injury site (Fig. 4C). Pooled data from five experiments demonstrated the significant reduction of NeuN-positive cells at the injury site (T9–T11, centered at T10) compared to rostral (T9–T6) and caudal (T11–L1) segments ($P < 0.001$, ANOVA followed by Tukey–Kramer all pairwise multiple comparisons test; see Fig. 4D).

This histological evidence describes a massive neuronal damage at the site of injury and proves the blockage at the impact site of electric signals that would have otherwise travelled along the spinal cord.

Spinal Cord Oxygenation Drops After a Spinal Impact

After an SCI, systemic hypotension and pericyte constriction of spinal capillaries decrease spinal oxygen delivery, reducing oxygen concentration on spinal tissues (Partida et al. 2016; Li et al. 2017; Williams et al. 2020). To quantify spinal cord oxygenation (SCO_2) during contusion, an intraparenchymal probe for O_2 was positioned 100 µm deep into the cord on the ventral funiculus between L1

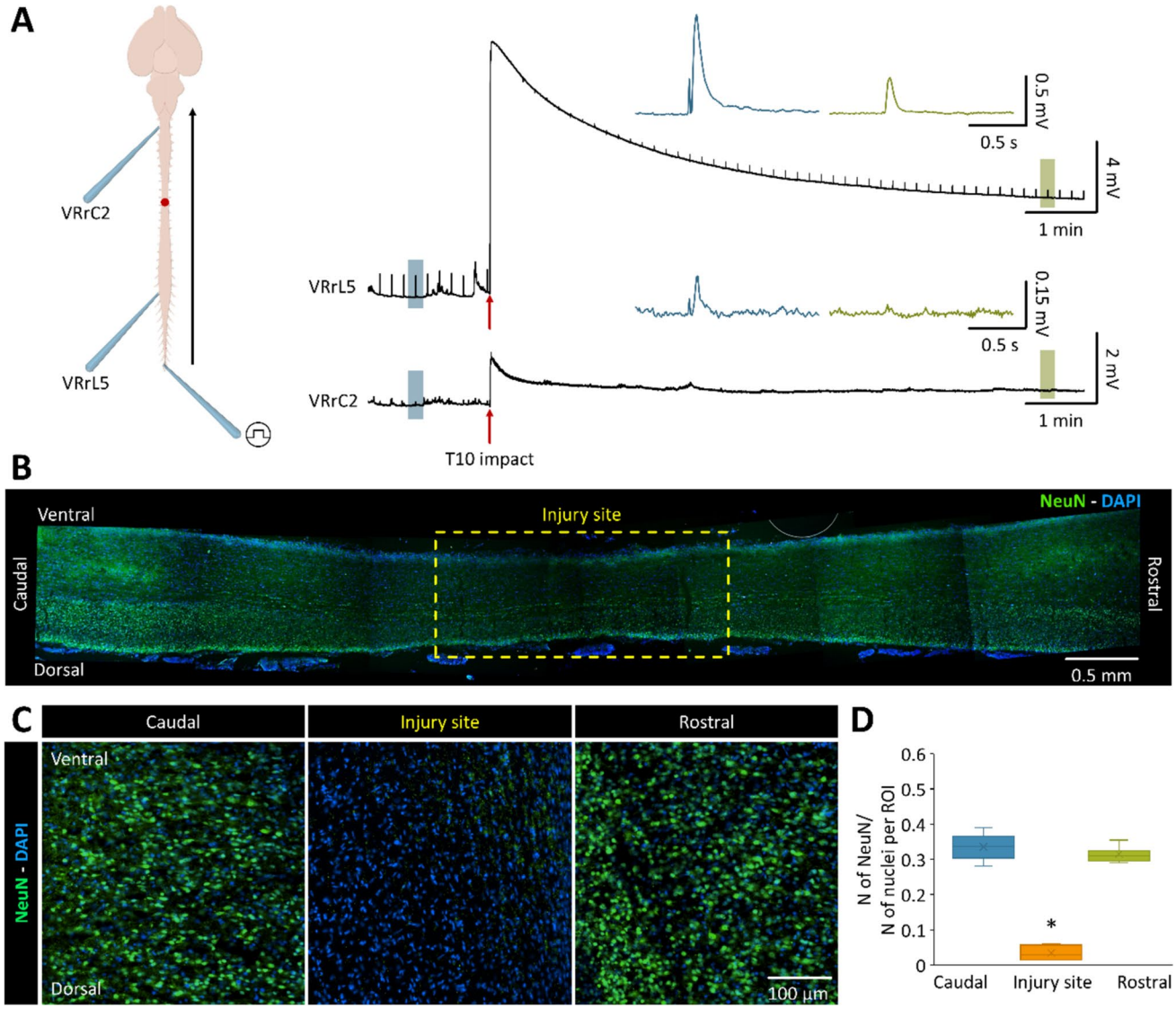

Fig. 4 Contusion suppresses ascending conduction of afferent input and causes massive neuronal death at the site of ventral impact. **A** The cartoon depicts the CNS preparation with the impact site on the ventral aspect of T10 (red dot). Extracellular electrodes are positioned at C2 and L5 rVRs, and repetitive electrical pulses (0.1 Hz, 100 µA, duration = 100 µs) are supplied to sacrocaudal to elicit ascending input (arrow). Right traces show simultaneous recordings from VRrL5 and VRrC2 with reflex responses appearing in control and magnified in the blue insert. After the depolarization induced by the impact (red arrow), evoked motor responses are abolished on both VRs. During repolarization, responses progressively reappear on lumbar VR, while lumbar reflexes become visible again after 38 s from the impact and recover towards the original size by the time (8 min, top green insert). Contrariwise, reflexes from VRrC2 do not recover (bottom green insert). **B** Reconstruction of sagittal tissue sections of a spinal cord (caudal left, rostral right, ventral up, dorsal down) as processed with DAPI and NeuN staining. A massive cellular loss is visible on the ventral aspect of the impact site. The base of the dotted yellow rectangle centered at T10, is calibrated to the width of the impactor tip. **C** Magnifications of sagittal tissue sections as in **B** stained with DAPI and NeuN, and collected from serial spinal segments at caudal level (T11-L1, left), injury site (T9-T11, centered at T10, middle) and rostral spinal cord (T9-T6, right). The lack of NeuN (green) staining at the site of impact indicates extensive neuronal loss. **D** The plot quantifies the statistical reduction of NeuN-positive cells at the injury site compared to both rostral and caudal segments (*$P < 0.001$, ANOVA followed by Tukey–Kramer all pairwise multiple comparisons test, $n = 5$). Cell count is normalized to the total number of nuclei in the region of interest (ROI)

and L2 VRs, while continuous electrophysiological signals were derived from VRrL1. The time course of average PO_2 from nine preparations indicated that SCO_2 in control (31.19 ± 7.36 Torr) dropped to 11.68 ± 4.03 Torr after the impact, and then slowly recovered to the 78.74% of control after 30 min (Fig. 5C).

SCO_2 for ex vivo preparations parallels the level of cellular activity as the induction of rhythmic locomotor-like

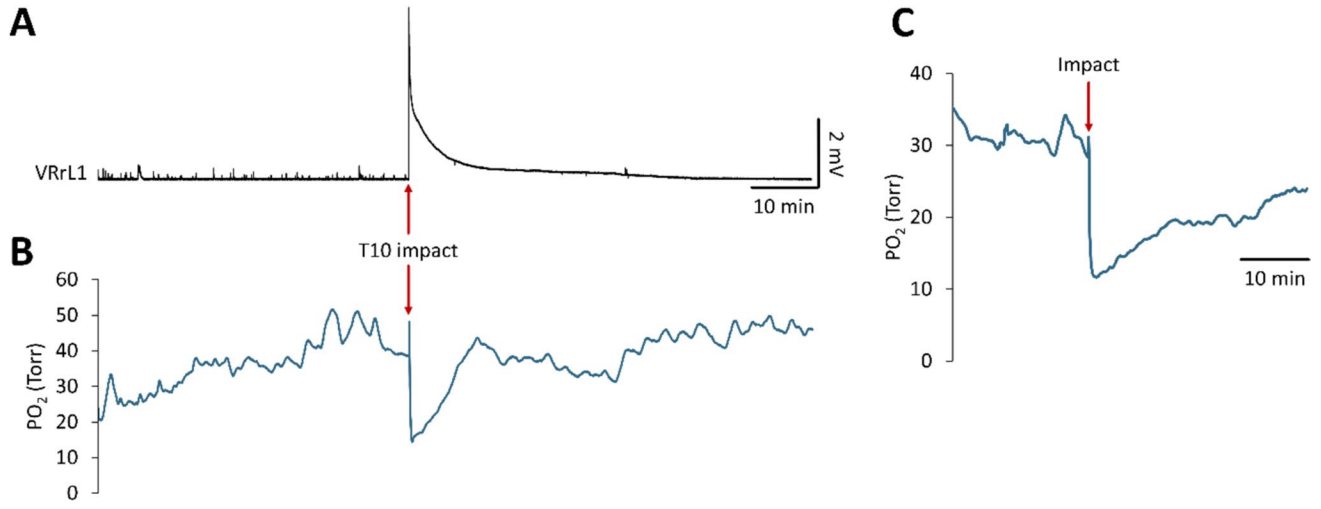

Fig. 5 Impact drops SCO_2 with a pattern that mirrors the profile of injury-induced depolarization. **A** Continuous trace from VRrL1 with a large depolarization at the site of impact at T10 (red arrow, 5.23 mV), which recovered to baseline after 12 min. **B** Simultaneous SCO_2 measurements performed from the ventral funiculus between L1/L2 VRs in the same experiment as in A, with PO2 values oscillating between 20.44 and 50.91 Torr in control. PO_2 drops right after the impact (8.12 Torr), eventually recovering to baseline after 10 min, mirroring the profile of DC level changes in **A**. **C** Average spinal PO_2 profile before and after the impact (red arrow, $n = 9$)

activity corresponded to a fall in tissue PO_2. (Wilson et al. 2003). To provide a reference for SCO_2 during a large depolarization, the CNS was perfused for 10 min with a modified Krebs solution containing 10 mM KCl. Potassium induced a mean depolarization of 1.83 ± 0.54 mV from VRL1, while average PO_2 measured from the L1 spinal segment dropped to 9.54 ± 2.14 Torr (SI. Fig. 2A).

The link between the increased neural activity induced by a large depolarization and the PO_2 drop was further explored using a CNS preparation that underwent a functional inactivation through heat-shock (100 °C) and then a continuous perfusion with oxygenated Krebs. Here, no depolarization was recorded from VRrL5 after exposure to potassium (10 mM), while an intraparenchymal probes for O_2 inserted at L1 spinal level derived a mean PO_2 of 528 ± 8.74 Torr equal to pre-K^+ control values. In the same preparation, the spinal impact did not elicit any depolarizations from VRrL5, with PO_2 measurements that remained unchanged before and during the impact (505.76 ± 2.57 in control and 508.75 ± 3.16 Torr during impact, SI. Fig. 2C).

Collectively, the impact induced a drop in SCO_2 that mirrors the kinetics of impact-induced depolarization and was comparable to the activation of spinal networks following 10 mM K^+.

Impact Transiently Suppresses Lumbar Motor Reflexes

A compression of the spinal cord is followed by a spinal shock, characterized by the suppression of motor evoked responses below injury, lasting beyond the moment of the first insult (Ditunno et al. 2004). To confirm the presence of a shock phase in our ex vivo SCI model, stimuli were continuously supplied to sacrocaudal afferents (frequency = 0.1 Hz, intensity = 1.6–6.15 Th, pulse duration = 0.1 ms) while motor reflexes were derived from VRrL5 in control (peak amplitude = 0.77 ± 0.2 mV). The profile representing changes in the amplitude of reflex responses throughout the experiment displays a complete suppression of motor reflexes in correspondence to a localized impact at T10 (red arrow, Fig. 6A, B). The transient disappearance of lumbar motor reflexes after trauma at T10 was obtained in five preparations where reflexes were also halted at the early peak of the depolarization evoked by 10 mM K^+. After 27.91 ± 6.06 s from the impact, smaller electrically evoked responses reappeared, and recovered to 90% of pre-impact values after 18.25 ± 12.2 min. In the same five preparations, the time of reappearance of the first reflex after impact was not correlated to the amplitude of the injury potential (correlation coefficient = −443, $P = 0.455$). Through multiple simultaneous recordings, comparable transient suppressions of motor reflexes were reported across VRs at spinal segments L1, L2, L4, L5, L6 on both sides. To exclude that the transient halt of lumbar reflexes is due to an interference produced by the impactor movement, in one sample, lumbar responses were allowed to recover after being transiently abolished by a first impact at T10. Then, the spinal cord was completely transected at L1 level (SI. Fig. 5A, B) and, after at least 15/20 min, a second impact at T10 was performed, which did not evoke any injury potentials from the disconnected caudal cord nor varied the amplitude of reflex responses

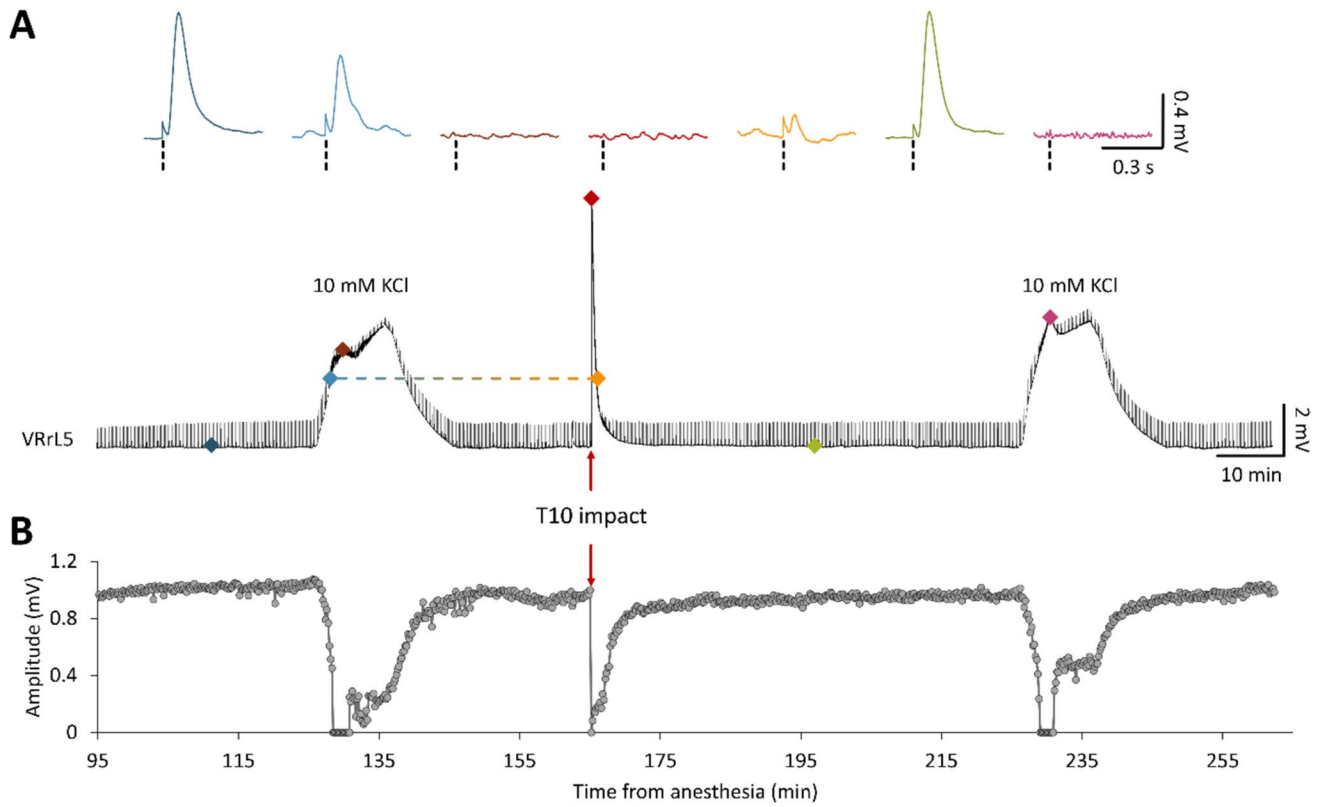

Fig. 6 Motor reflexes vanish at the peak of both, chemically- and impact-induced depolarizations. **A** A 178 min long recording from VRrL5 during the continuous delivery of electrical pulses to sacrocaudal afferents (frequency = 0.1 Hz; intensity = 100 µA, 5 × Th; pulse duration = 0.1 ms) to evoke motor responses. Motor reflexes are traced in control, during 10 mM K^+ perfusion, wash out, impact to T10 (red arrow) and a second K^+ application. The first exposure to K^+ elicits an early depolarization of 4.05 mV and suppresses reflexes, which recover to baseline during washout in normal Krebs. Afterwards, at the peak of the impact-induced depolarization (9.69 mV), motor evoked responses are transiently suppressed but fully recover, as the baseline repolarizes, after 31.06 min from the impact. A second exposure to 10 mM K^+ evokes an early depolarization of 4.55 mV, which abolishes motor reflexes until their full recovery during washout. Top inserts magnify single reflexes (dotted vertical lines correspond to artifacts of stimulation) for distinct instants of the experiment as indicated by the colored dots below. At the top of each depolarization, motor reflexes are suppressed (brown, red and purple top traces). **B** Time course of reflex amplitude for the trace in **A** demonstrates that reflexes vanish (amplitude = 0 mV) during sudden depolarizations elicited by either perfusing the entire CNS with potassium or by applying a localized impact to the cord

(SI. Fig. 5B). Noteworthy, the second impact still elicited an injury potential from the rostral cord (SI. Fig. 5B).

In summary, in the current study, the calibrated and localized impact to the cord has always been followed by a transient suppression of evoked reflexes from spinal motor pools.

A Thoracic Impact Alters electrically induced Fictive Locomotor Patterns

Results collected so far indicate that, after an impact, the entire spinal cord experiences a transient large depolarization, with neuronal death only at the injury site. To explore whether the depolarization induced by the impact affects the functionality of lumbar spinal networks for locomotion, stereotyped trains of rectangular pulses (frequency = 2 Hz, intensity = 1–5 × Th, pulse duration = 0.1 ms) were applied to sacrocaudal afferents for 80 s (Fig. 7 A). In response to stimulation, episodes of locomotor-like oscillations were recorded in control and at different time points after the impact (15, 60, and 120 min post-SCI, Fig. 7A, B). Signals characteristically appeared double alternating between flexor-related signals from VRL2 and extensor-related commands from VRL5, as well as between left and right motor pools (Kiehn and Kjaerulff 1996). Pooled data from seven experiments showed that the impact unaltered several characteristics of fictive locomotion (SI. Fig. 6) but did reduce cumulative depolarization (Fig. 8A; $P = 0.002$, repeated measures ANOVA followed by Dunnett multiple comparisons test vs ctrl, $n = 6$) and amplitude of cycles from VRrL2 (Fig. 8B; $P < 0.001$, repeated measures ANOVA followed by Dunnett multiple comparisons test vs ctrl, $n = 6$). In addition, duration of fictive locomotion episodes from VRrL2 after 60 min from the impact (Fig. 8C; $P = 0.031$, repeated

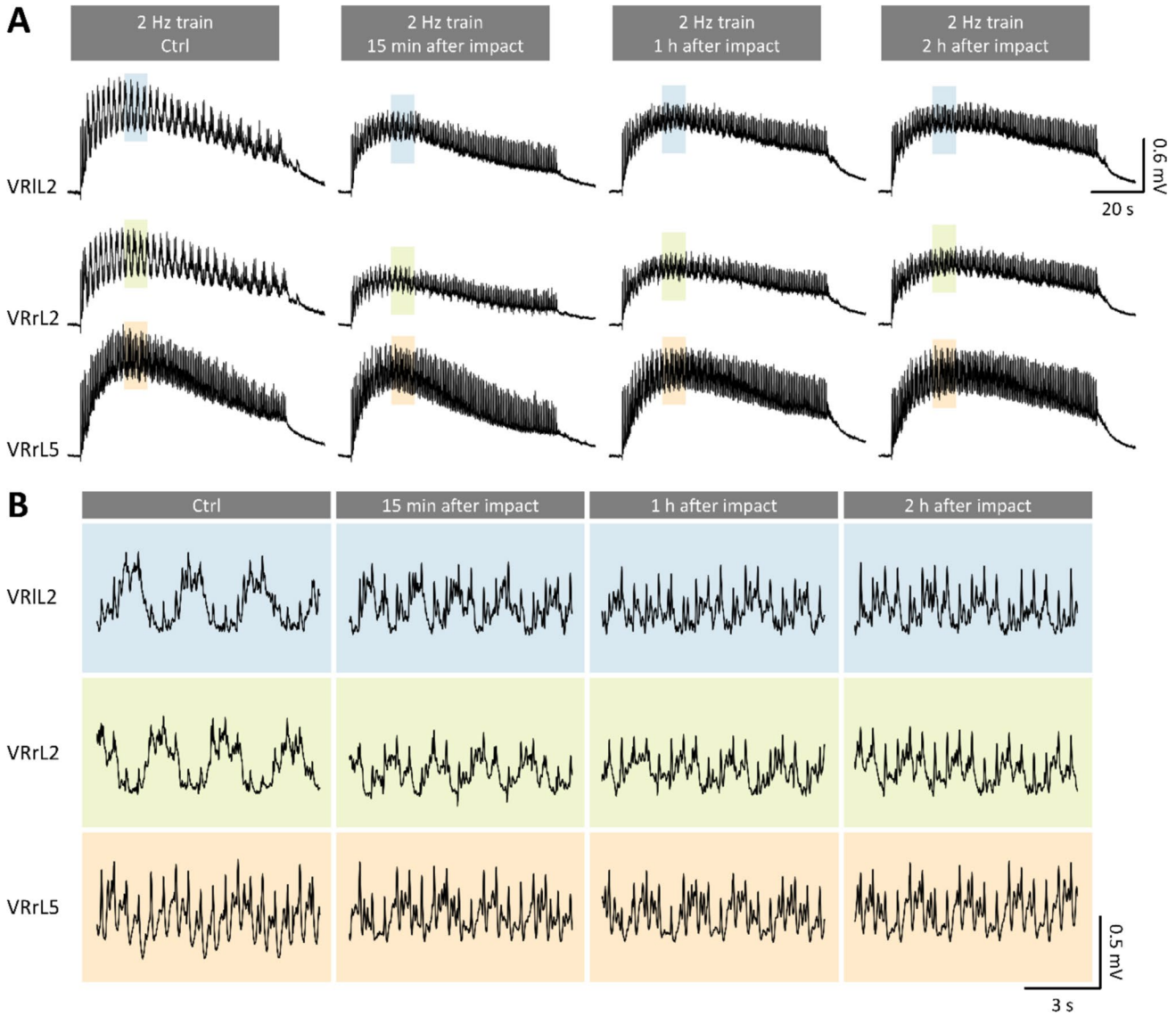

Fig. 7 electrically induced fictive locomotion is affected by a localized thoracic compression. **A** Serial 2 Hz trains of stereotyped rectangular pulses (intensity = 125 µA, duration = 0.1 ms) are applied to sacrocaudal afferents to evoke epochs of locomotor-like oscillations from VRlL2, VRrL2, and VRrL5. Fictive locomotion patterns were recorded in control, and then 15 min, one hour, and two hours after injury. Fictive locomotor patterns recorded in control from VRrL2 were characterized by a cumulative depolarization of 0.7 mV with 28 superimposed alternating cycles (homolateral CCF = − 0.70, homosegmental CCF = − 0.87), defined by a peak amplitude of 0.33 ± 0.08 µV and a period of 2.89 ± 0.74 s. In the same preparation, impact reduced cumulative depolarization (0.5 mV, 15 min post-SCI), generating smaller (0.16 ± 0.06 µV, 15 min post-SCI) and slightly less regular locomotor-like oscillations (period CV = 0.28, 15 min post-SCI Vs. period CV in control = 0.26), regardless their unchanged number (28, 15 min post-SCI). **B** Magnifications of simultaneous traces (blue fields for VRlL2, green for VRrL2, and orange for VRrL5) correspond to oscillations captured at steady state in **A** (shaded rectangles). Note the out-of-phase cycles recorded from the three VRs, with reduced amplitude and periodicity after the impact

measures ANOVA followed by Dunnett multiple comparisons test vs ctrl, $n = 7$), and period of cycles of VRrL2 after 15 and 60 min from the impact, were significantly lower than in control (Fig. 8D; $P = 0.008$, repeated measures ANOVA followed by Dunnett multiple comparisons test vs ctrl, $n = 7$). Similarly, 15- and 60-min post-impact, episodes from VRrL5 were faster than in the control group (Fig. 8E; $n = 6$, $P = 0.002$, Friedman test followed by Dunn's multiple comparisons test vs ctrl), as well as more irregular at 15 min post-impact (Fig. 8F; $P = 0.006$, repeated measures ANOVA followed by Dunnett multiple comparisons test vs ctrl, $n = 7$). Notably, after injury, oscillations from both extensor and flexor commands (Fig. 8G; homolateral CCF, $P = 0.013$, repeated measures ANOVA followed by Dunnett multiple comparisons test vs ctrl, $n = 7$), as well as from the left and right sides of the cord (Fig. 8H; homosegmental CCF,

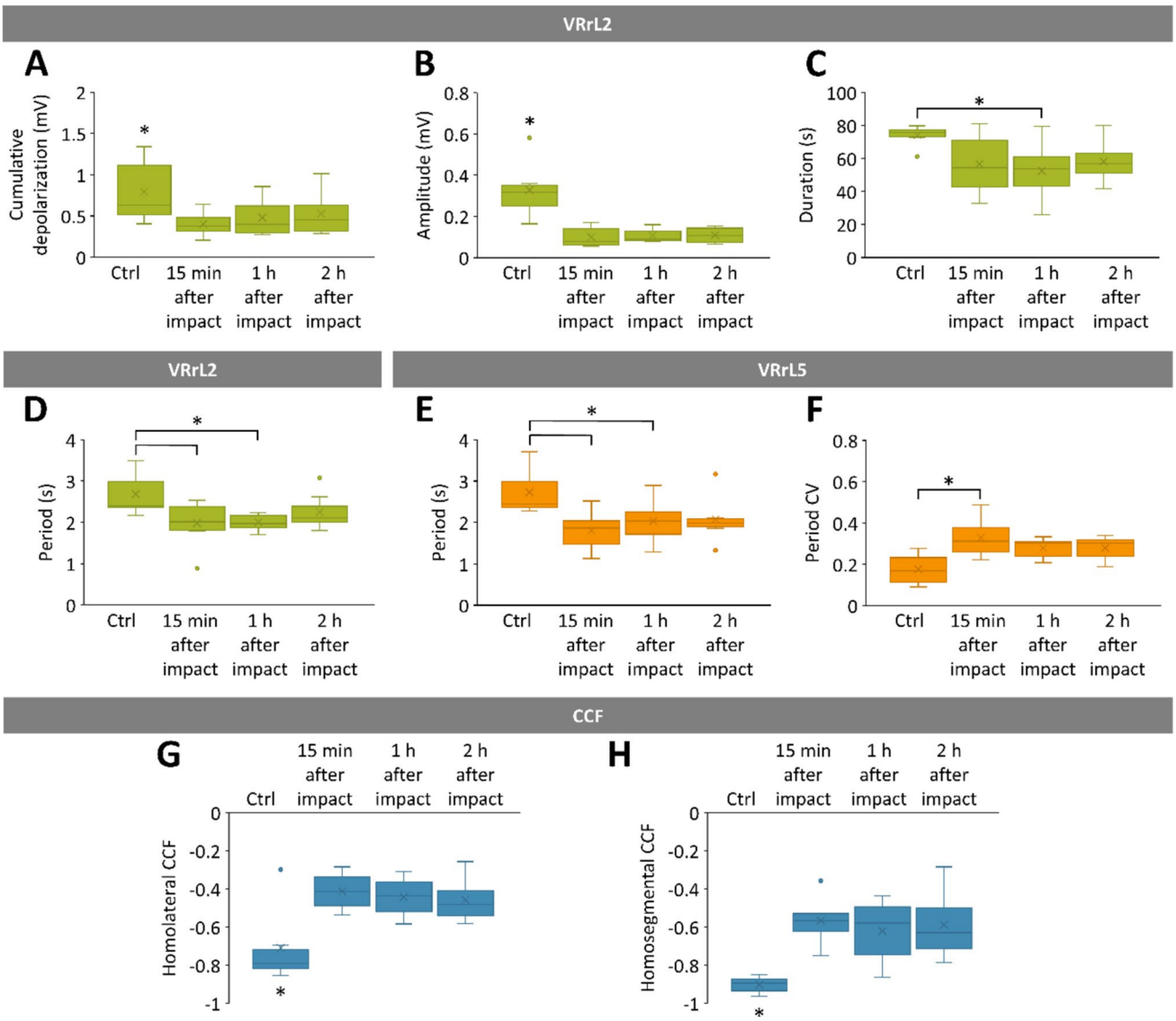

Fig. 8 Impact perturbs the features of electrically induced fictive locomotion. **A–D** Green box-and-whisker plots describe average values for the main descriptors of fictive locomotor patterns reported from VRrL2 in control and at 15 min, 1 h, and 2 h following the injury. **A** Cumulative depolarization significantly decreases after impact (*$P=0.002$, repeated measures ANOVA followed by Dunnett multiple comparisons test vs ctrl, $n=6$). **B** Impact largely reduces the amplitude of oscillations (*$P<0.001$, repeated measures ANOVA followed by Dunnett multiple comparisons test vs ctrl, $n=6$). **C** Episodes of fictive locomotion are shorter one-hour after the impact (*$P=0.031$, repeated measures ANOVA followed by Dunnett multiple comparisons test vs ctrl, n = 7). **D** Period of oscillations is significantly smaller 15 min and one-hour post-impact (*$P=0.008$, repeated measures ANOVA followed by Dunnett multiple comparisons test vs ctrl, $n=7$). **E** and **F** Orange box-and-whisker plots describe values for the main descriptors of fictive locomotor patterns reported from VRrL5 in control and at 15 min, 1 h, and 2 h following the injury. **E** Periods of fictive locomotion (FL) oscillations 15 min and one hour after injury are significantly shorter than in the control group (*$P=0.002$, Friedman test, $P=0.002$). **F** Period CV is higher than in control only at 15-min post-injury (*$P=0.006$, repeated measures ANOVA followed by Dunnett multiple comparisons test vs ctrl, $n=7$). **G** Phase coupling between extensor and flexor commands (homolateral CCF, *$P=0.013$, repeated measures ANOVA followed by Dunnett multiple comparisons test vs ctrl, $n=7$) is poorer after the impact. **H.** Phase coupling between the left and right output (homosegmental CCF, *$P=0.001$, repeated measures ANOVA followed by Dunnett multiple comparisons test vs ctrl, $n=7$) reduces post injury

$P=0.001$, repeated measures ANOVA followed by Dunnett multiple comparisons test vs ctrl, $n=7$) exhibited poorer alternating coupling than controls.

In summary, a calibrated impact to the thoracic cord affects the functionality of lumbar locomotor circuits, generating less coordinated locomotor-like oscillations, with shorter and faster cycles of locomotor-like patterns especially from flexor motor pools.

Impact-Induced Depolarization is Sustained by Chloride Ions

To investigate whether ionic disbalances sustain the depolarization that follows the impact, separate experiments considered injuring the cord during perfusion with either of the three modified Krebs solutions containing low concentrations of chloride (Cl^-), calcium (Ca^{2+}), and potassium (K^+) ions, respectively. Continuous recordings were performed from preparations initially perfused with normal oxygenated Krebs solution, and then with one of the low-ion Krebs solutions for 30–90 min before the impact and for 15 min afterwards. As soon as a single low-ion solution was applied, the DC level of the baseline recorded from VRrL5 hyperpolarized and, after 18 min, reached a steady-state mean level of -10.42 ± 2.23 mV for low Cl^- (n = 5), -0.49 ± 0.39 mV ($n = 7$) for low Ca^{2+} and -1.11 ± 0.75 mV for low K^+ ($n = 7$; SI. Fig. 7).

Whether low-ion solutions affected spinal synaptic transmission was verified by continuously monitoring the reflex responses elicited from VRrL5 in response to trains of weak electric pulses (frequency = 0.1 Hz, intensity = 50–160 µA, 2–8 × Th) applied to sacrocaudal afferents (Fig. 9A). Pooled data from many experiments confirms that the peak of mean reflexes was unchanged by low Cl^- ($P = 0.923$, paired *t*-test, $n = 6$), while it significantly reduced after low Ca^{2+} ($37.80 \pm 7.76\%$ of control; $P < 0.001$, paired *t*-test, $n = 7$) and it increased with low K^+ ($113.34 \pm 11.38\%$ of control; $P = 0.017$, paired *t*-test, $n = 7$; Fig. 9B). Conversely, latency of responses was only affected by the transition to the low Cl^- solution ($109.96 \pm 3.75\%$ of control; $P = 0.001$, paired *t*-test; Fig. 9C, left) without any changes appearing with low Ca^{2+} ($P = 0.069$, paired *t*-test, Fig. 9C, middle) or low K^+ ($P = 0.297$, paired *t*-test; Fig. 9C, right).

Impacts occurring during perfusion with low-ion solutions generated different peaks and profiles of injury-induced potentials. Comparison between three mean traces recorded for up to 3.5 min after the impact (red arrows) demonstrates that low Cl^- concentrations ($n = 6$, Fig. 9D, left) generate higher peaks of injury potentials compared to the other two modified Krebs solutions. Furthermore, despite a lower peak of depolarization, low Ca^{2+} broadened the average injury potentials with the appearance of a delayed component in the repolarizing phase ($n = 7$; Fig. 9D, middle). Low K^+ perfusion showed a peak similar to low Ca^{2+} depolarizations, but with a sharper repolarizing phase ($n = 7$; Fig. 9D, right).

Comparison among the mean amplitude of injury potentials generated by the impact during perfusion in normal Krebs (5.46 ± 3.54 mV; $n = 23$) and in the presence of the three low-ion solutions indicated a significantly higher depolarization for impacts occurring in low Cl^- (10.56 ± 3.57 mV, $P = 0.048$, Kruskal–Wallis test followed by Dunn's all pairwise multiple comparisons test, $n = 6$, Fig. 9E). Nevertheless, after impact in low Cl^-, reflex responses were suppressed with a time course reminiscent of post-injury reflexes in normal Krebs solution, with a first reappearance of responses after 20.64 ± 6.15 s from the impact and the recovery to 90% of pre-impact values after 11.08 ± 4.61 min.

Impacts in the presence of the modified Krebs solutions revealed the distinct role of Cl^- ions in sustaining the extent of injury potentials, albeit the duration of spinal shock and the suppression of reflex responses were comparable among the different media.

Discussion

The current study is centered around tracing the immediate consequences of a traumatic injury to the spinal cord. For the purpose, we designed a novel experimental platform composed of a classical electrophysiological set up for multiple and simultaneous nerve recordings and stimulation, combined with an oximetric implantable probe, and associated with the invention and use of an ad hoc low-noise mini-impactor. This experimental infrastructure has been tailored to best exploit the innovative version of the whole CNS isolated from neonatal rats we recently introduced (Mohammadshirazi et al. 2023). To provide a more physiological and stable site for a traumatic impact, we adopted a more conservative surgery that maintained dorsal vertebral laminae and DRG mostly intact. The impactor was carefully shielded to simultaneously allow VR recordings, and was created as to allow consistent and calibrated focal impacts through a fully programmable software interface. Each impact triggered a transient and massive depolarization spreading from the injury site to the whole spinal cord, symmetrically propagating across the left and right sides of the cord, and also to the dorsal cord, although with smaller and slower potentials than the ventrally elicited ones. Several fundamental features of the pathophysiology of a severe acute SCI were reproduced in our experiments, such as: (1) an extensive neuronal loss at the site of injury, with a transient drop in SCO_2; (2) a complete functional interruption of longitudinal input at the level of impact with a disconnection of the sublesional lumbar cord from descending motor commands; and (3) a momentary suppression of evoked spinal reflexes. Additionally, our setting highlighted the disappearance of the spontaneous motor activity that is characteristically recorded from the spinal VRs of preparations isolated from newborn rats, showing a drop in the excitability of sensorimotor networks, resembling the flaccid muscle tone displayed in clinics during a spinal shock.

As opposed to the massive neuronal loss at the site of injury, the number of sublesional lumbar motor pools quantified by NeuN and SMI 32 did not undergo any changes,

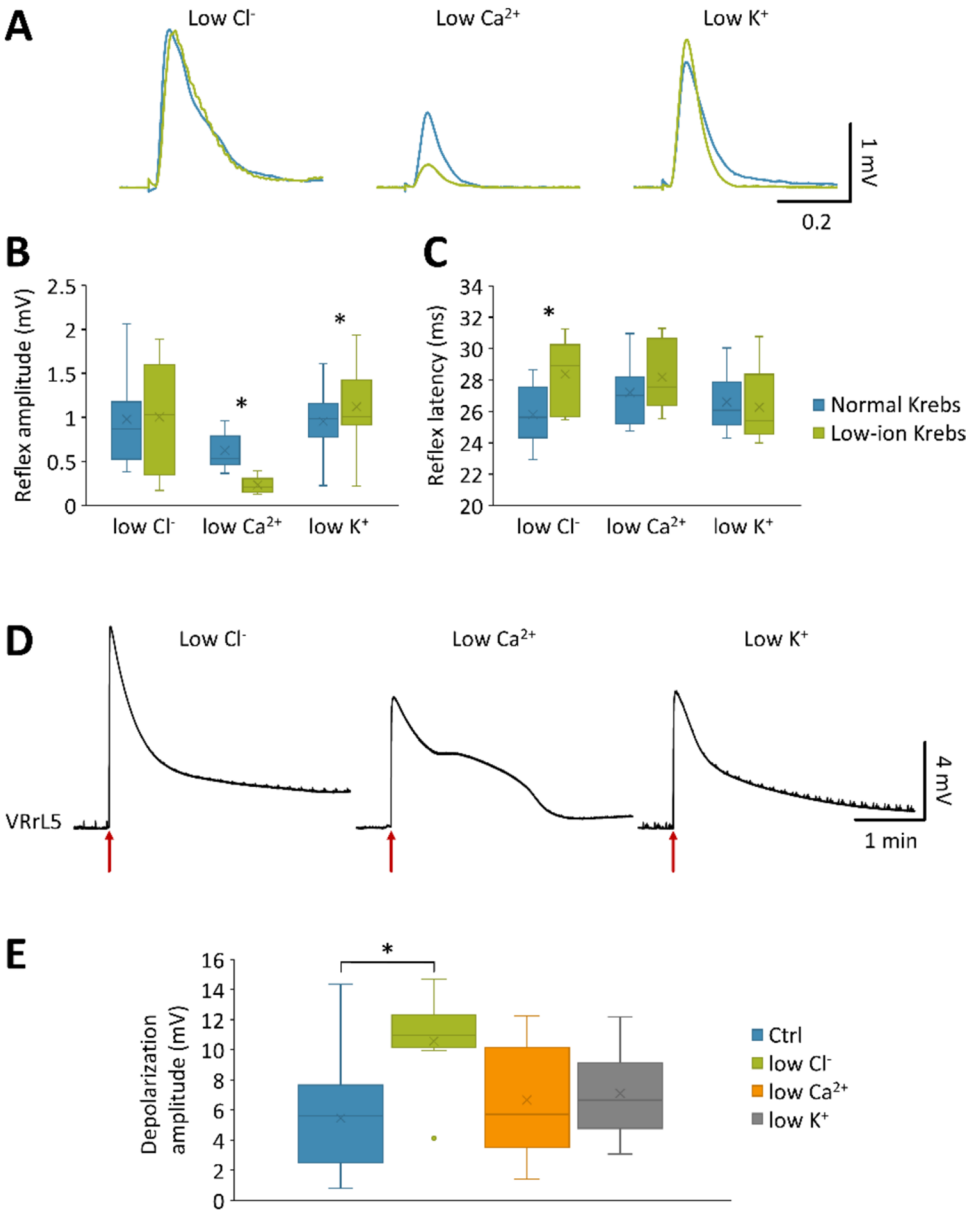

Fig. 9 Low-ion solutions differently influence synaptic transmission and impact-induced depolarization. **A** Three superimposed pairs of electrically induced reflex responses from three different preparations representing transition from normal Krebs solution (blue traces) to modified Krebs solutions (green traces) with low Cl^- (left), low Ca^{2+} (middle), and low K^+ (right) concentrations. Notably, compared to normal Krebs solution, the peak of responses remained unchanged during perfusion with low Cl^- (left), while perfusion with low Ca^{2+} solution (middle) reduced the peaks to 30.69% and transition to low K^+ (right) augmented peaks to 117.88% of Krebs'. **B** Mean amplitude of reflex responses in normal Krebs (blue box-and-whisker plots) or low-ion solutions (green box-and-whisker plots) point out a significantly smaller peak during application of low Ca^{2+} ($P<0.001$, paired *t*-test, $n=7$), and a higher amplitude after transition to low K^+ ($P=0.017$, paired *t*-test, $n=7$) solutions. **C** Mean values of latency of reflex responses in normal Krebs (blue box-and-whisker plots) and low-ion solutions (green box-and-whisker plots) report significantly slower responses when the low Cl^- solution is perfused ($P=0.001$, paired *t*-test). **D** Four-minute traces from VRrL5 related to the average profiles of injury potentials during perfusion with low-ion solutions (left, low Cl^-, $n=6$; middle, low Ca^{2+}, $n=7$; right, low K^+, $n=7$). **E** Average peak amplitude of impact-induced depolarizations during perfusion in control Krebs and low-ion solutions. Low Cl^- solution augments the amplitude of depolarization (*$P<0.05$, Kruskal–Wallis test followed by Dunn's all pairwise multiple comparisons test, $n=6$)

while the functionality of locomotor networks was slightly affected, even after two hours from the impact, showing less coordinated locomotor-like cycles, especially from flexor motor pools. Interestingly, after SCI, tail flexor motoneurons underwent distinct morphological alterations, such as a reduction in soma size and an overall decrease in dendritic

branching, which concur to the development of spasticity in chronically injured animals (Kitzman 2005). These morphological changes parallel the selective expression of GABA receptor subunits for flexor, but no extensor, motoneurons in chronic paraplegic rats with a spinal transection during the first postnatal week (Khristy et al. 2009). Similarly, in paraplegic patients, the appearance of spasms is associated with the exaggerated appearance of flexor reflexes (Hiersemenzel et al. 2000).

In our experiments, the large depolarization triggered by the trauma was further broadened by the low extracellular concentrations of calcium ions, which facilitate the extrusion of calcium from injured spinal cells. This observation confirms the well-known massive calcium release during acute SCIs (Young and Koreh 1986). Surprisingly, we discovered a crucial role for the rapid outflow of chloride ions in sustaining injury potentials immediately after trauma, as we noticed a maximal depolarization upon increasing the driving force for chloride ions. To the best of our knowledge, this is the first time that chloride ions have been linked to the initial response triggered by a physical trauma to the spinal cord. This evidence could be pivotal in deciphering the origin of the dysregulation of intracellular chloride concentrations that sustain spasticity in persons with chronic SCI.

A Novel Ex Vivo Model to Trace the Immediate Consequences of a Physical Injury to the Spinal Cord

Starting from the pioneering device introduced by Allen (Allen 1911), several variations of the original weight drop impactor have been proposed (Wrathall et al. 1985; Kwo et al. 1989) and adopted worldwide, with a standardization for adult rodents (Young and Bracken 1992; Basso et al. 1996). These resources had a tremendous impact on current knowledge about SCI, but several features of the technique inherently move the outcomes of these experimental injuries far from a clinical scenario. First of all, ethics requires animals to be fully anesthetized, inevitably affecting the composition of spinal tissue (Salzman et al. 1993; Robba et al. 2017; Davis and Grau 2023). Secondly, breathing chest movements and heartbeat contribute to uniquely vary inter-animal conditions at the time of injury, hence limiting the consistency of the outcome produced by any two identical injury paradigms. Furthermore, the technique only allows a dorsal injury, avoiding the challenging surgical procedures required to transiently move the trunk internal organs to have access to the ventral cord. Hence, it is impractical to replicate a ventral SCI, which is a widely spread condition in clinical epidemiology (Ahuja et al. 2017). Last but not least, currently available impactors generate mechanical and electrical interferences, that come from either the engine or the piston that drives the rod's vertical displacement, jeopardizing any simultaneous electrophysiological recordings close to lesion site. Our system overcomes all mentioned weaknesses, albeit limited to basic research investigations using ex vivo tissue isolated from newborn rodents. Our approach is not intended to replace preclinical tests for the translation of novel treatments in clinics, but to offer an optimal complementary step to challenge innovative basic ideas to target the immediate consequences of a physical injury to the nervous tissue. Our platform is unique in tracing the events at the base of a spinal shock, a topic that has been quite forsaken among the vast SCI research. The constraint of using immature tissue, because of its optimal ex vivo survival, hinders highly detailed studies on the physiopathology of adult SCIs, but opens up to the investigation of the still underexplored field of pediatric injuries (Carreon et al. 2004).

In addition, some ex vivo models have been defined to explore the mechanical stimulation of the CNS, studying axonal mechanobiology and neuronal membrane deformations, using stretch forces (Aomura et al. 2016) or shear strains (LaPlaca et al. 2005; Bottlang et al. 2007) on cell cultures, and on organotypical or acute CNS tissue sections. While these techniques trace the molecular dynamics at single cell level after mechanical forces have been applied, they cannot pair the informative content of simultaneous electrophysiological recordings. On the other hand, our calibrated microimpactor applies even sudden and orthogonal compressive forces to the nervous tissue of an isolated preparation of the entire CNS, that maintains the multifaced composition of the distinct neural structures. Notably, the low noise design of the device and the stability of the preparation at the impact site allows continuous and stable DC recordings even at the time of impact, with no artifact that prevents signal acquisition after the impact. Based on the most updated literature, no other electrophysiological setups are currently available to record spinal potentials, apart from one attempt that provided recordings after more than 4 min from the impact and after electrodes had been replaced and repositioned, hence limiting the reliability of internal pre-injury controls (Goodman et al. 1985).

Overall, we are aware that our neonatal SCI model ex vivo is very different from in vivo preparations. In comparison with preclinical SCI models, it avoids anesthesia and increases stability of tissues during recordings. However, dissection of the entire CNS from a pup inevitably severed all peripheral (cranial + spinal) nerve roots, which is per se a kind of peripheral nerve injury. Secondly, since the dissection lasts 20–25 min, followed by incubation in Krebs solution for a few hours, neuronal excitability could be compromised to a certain extent. Indeed, although the Krebs solution provides the necessary nutrition and oxygen to the tissue, the relatively thin tissue may not allow nutrition to equally penetrate all districts of the CNS, likely causing changes in the excitability of neurons in different regions (Wilson et al. 2003). Besides their intrinsic limitations,

isolated preparations have been extremely useful to trace the functional organization of spinal networks for locomotion in mammals (Kjaerulff et al. 1994; Whelan et al. 2000; Marchetti et al. 2001) and still represent a worthwhile experimental tool for elucidating the intricate functional organization of spinal networks for locomotion (Hsu et al. 2023). Similar studies can now be implemented using our experimental platform to further investigate neuronal plasticity during development, associated to a calibrated injury.

Neuronal Source of Injury Potentials Acquired in the Current Study

The main concern of any well-educated electrophysiologists is the certainty of the genuine biological origin of any acquired signals, to exclude any confounding baseline drifts due to environmental interferences or electromechanical artifacts from the equipment of electrophysiological set-ups. That said, albeit the presence of injury potentials triggered by a physical injury to the cord has already been reported (Goodman et al. 1985; Wang et al. 2015), we wanted to verify the nature of the large depolarization we recorded about 200 ms after the impactor starts lowering. Noteworthy, the device was carefully designed, fabricated, and tested to minimize any sources of electromagnetic emissions, which are stereotyped and instantaneous at the moment of activation.

We collected several convincing proofs about the spinal origin of the potentials we acquired during impact delivery. Namely, we observed that: (1) potentials occur with a latency of hundreds of milliseconds from the onset of both, engine activation and actual physical strike to the cord; (2) while artifacts are synchronous across all recording sites, the potentials we derived from VRs own different latencies and slower potentials the farther we moved from the impact site; (3) similarly, derived potentials propagate ventro-dorsally, appearing on DRs only after homologous VRs; (4) motor reflexes are suppressed at the top of each potential, and they gradually recover during baseline repolarization, similarly to the reappearance of motor reflexes washing out from 10 mM K^+ concentrations; (5) the injury potential pairs with a reduction in SCO_2; (6) amplitude and profile of potentials are modulated in the presence of modified ion solutions.

Additionally, we designed several experimental protocols to confirm that the large deflection of DC level following the impact corresponds to a real neuronal potential, and it is not the mere result of either the engine interference, mechanical movements produced, or the quick displacement of the tip in the bath. Thus, tests aimed at proving that: (I) when the device was activated in the bath close to the preparation, but without touching the cord, no baseline drifts were produced; (II) when serial impacts of equal severity were applied to the same site, the peaks of potentials remained stable, hence excluding any summation of artifacts; (III) no potentials were recorded when the device acted on a preparation that was already largely depolarized by high K^+ concentration (50 mM); (IV) no DC deflections were recorded when the impact was inflicted to a heat-inactivated anoxic spinal cord; (V) the injury-related potential was lost when a second impact was inflicted after complete disconnection of the lesion site from the recording VRs. This convincing evidence proves that potentials recorded in correspondence to the activation of the impactor are not artifacts driven by the device engine, nor by the movement of the tip in the recording chamber filled with Krebs medium. Interestingly, the novel platform we introduced allows to elicit and quantify true injury potentials, making it a reliable and consistent tool to study spinal mechanobiology ex vivo.

Nature of an Injury-Induced Depolarization Spreading Along the Spinal Cord

The injury-induced depolarization was recorded first and with higher values in segments closer to the site of injury, and then spread both, rostrally and caudally, at the same speed. How this wave of excitation travels along the entire spinal cord is still to be clarified. However, conduction of injury potentials along the cord (0.03 ± 0.01 m/s) recorded in our study was ten times slower than spinal input conduction in the same preparation (from 0.2 to 0.4 m/s; Mohammadshirazi et al. 2023), hence excluding injury potentials being electrically conducted through longitudinal axons. In addition, conduction of injury potentials along the cord did not slow down in the presence of low Ca^{2+} concentrations (data not shown, 0.03 ± 0.01 m/s), which depress synapses, hence excluding a main role of wired transmission. Contrariwise, the delayed extrasynaptic volume transmission (Taber and Hurley 2014) through the extracellular space and the spinal canal (Agnati et al. 2010) would better account for a passive conduction of ions. In this case, ions sustaining the injury-induced depolarization flow through the cord under the pressure exerted by the smashed site of impact, just as squeezing the middle of a tube filled with saline solution would augment fluid pressure and movement of salts towards extremities. Perspective studies using selective pharmacological agents may target distinct membrane pore structures (e.g. ion channels, gap junctions, ionotropic receptors) that could be involved in the conduction of injury potentials.

Chloride Surge After a Traumatic Injury to the Cord: A Potential Link to Clinical Spasticity

The insurgence of spasticity-like behaviors in SCI rodents has been convincingly attributed to a dysregulation of intracellular chloride concentrations (Boulenguez et al. 2010; Mazzone et al. 2021), with a reduced expression of the membrane carrier KCC2, which co-transports

potassium and chloride outside the cell (Boulenguez et al. 2010). However, how an SCI affects chloride exchange in spinal neurons is still to be clarified. The current study suggests that a large chloride conductance sustains the early depolarization that follows a physical injury to the spinal cord. Indeed, the peak of potential was higher for impacts occurring in a low-chloride modified medium, which increases the driving force of inward chloride currents (Takahashi 1990). We hypothesize that the immediate overflow of chloride ions triggered by a physical injury to spinal tissue sustains a surge of extracellular chloride concentrations, possibly reversing the equilibrium potential of chloride ions. Starting from this early excitatory phase, the net movement of chloride ions across the membrane of spinal neurons possibly still remains perturbed throughout the chronic phase, leading the development of spasticity. Moreover, our results show both, a stable suppression of spontaneous motor activity from VRs and a transient phase of areflexia, right after the impact, followed by a gradual recovery of reflex responses during the following repolarizing phase. However, since motor reflexes consistently reappeared after a fixed amount of time from the impact, regardless of the extent of injury-induced depolarization and of the low concentration of extracellular chloride ions, it can be assumed that reflex depression was not a mere consequence of the overflow of chloride ions triggered by the impact. Thus, network excitation due to the immediate depolarization might be contrasted in the early phases by a following large depression of network excitability that is not directly linked to the extent of the first depolarization. This network inhibition would deserve further pharmacological investigations. Later on, network hyperexcitability prevails and thus spasticity appears. However, time constraints related to our acute ex vivo model hindered the possibility to test the occurrence of any chronic spastic-like activity after injury. We are also aware that the neonatal spinal cord used in the current study still presents an immature and opposite reversed chloride gradient (Gao and Ziskind-Conhaim 1995). This latter feature, although far from adult physiology, makes the neonatal spinal tissue much closer to the extracellular environment after SCI, where the chloride equilibrium is reverted towards that of immature tissues (Lu et al. 2008). We speculate that, albeit spasticity clinically appears only later on, after the recovery from the spinal shock, the molecular elements at the base of spasticity, such as the dysregulation of intracellular chloride concentrations, already start hundreds of milliseconds after the onset of a physical injury to the cord. This hypothesis supports the rationale for introducing immediate pharmacological (Liabeuf et al. 2017; Marcantoni et al. 2020) or electrical (Mekhael et al. 2019; Malloy and Côté, 2024) interventions to neuromodulate the shift in chloride concentrations as an early treatment to alleviate the appearance of spasticity in chronic SCIs.

Conclusion

The present study offers a novel in vitro model of traumatic spinal cord injury in rodent neonates that mimics the symptomatology of a spinal shock after acute SCI, and allows to record an immediate depolarizing potential as soon as hundreds of ms after the onset of an impact. Injury potentials originate from the activation of spinal neurons and propagate rostrally and caudally in ventro-dorsal directions from the site of impact and evenly on both sides of the cord. Although not directly damaged by the impact, spinal networks for locomotion showed early functional impairments after a thoracic spinal lesion. The effect of low ion concentrations on the magnitude of injury potentials may suggest the involvement of chloride ions in the sequela of events following a physical trauma to the immature spinal cord.

Supplementary Information The online version contains supplementary material available at https://doi.org/10.1007/s10571-024-01516-y.

Acknowledgements GT is grateful to Mrs. Elisa Ius for her excellent assistance in preparing the manuscript and to John Fischetti for technical support in fabricating the impactor. We owe to Carmen Falcone for her valuable contribution to data discussion and manuscript reviewing. The study was supported by intramural SISSA grants through the 5xMILLE2020 framework.

Author Contributions GT contributed to the study conception and design. AM, GM, and GT performed experiments. Material preparation, data collection and analysis were performed by all authors. The first draft of the manuscript was written and illustrated by GT and AM. GM commented on previous versions of the manuscript. All authors approved the final manuscript.

Funding Funding was provided by intramural SISSA grants (Grant No. 5xMILLE2020).

Data Availability The datasets generated during and/or analyzed during the current study are available from the corresponding author on reasonable request. No datasets were generated or analysed during the current study.

Declarations

Competing Interests The authors have no relevant financial or non-financial interest to disclose. The impactor adopted in the study is currently being patented by SISSA and is available upon request. The authors declare no competing interests.

Ethical Approval The study was performed in line with the principles of the Italian Animal Welfare Act 24/3/2014 n. 26 implementing the European Union directive on animal experimentation (2010/63/ EU). The study complied with the ARRIVE guidelines. The animal protocol was approved by the Italian Ministry of Health with the notification. 22DAB.N.52 M dated Oct 30th, 2019, and approved by SISSA ACUC (OPBA) committee (verbale n.17/3019).

Consent to Participate All authors give their formal consent to participate to the present manuscript.

Consent for Publication All authors give their formal consent for the publication of the present manuscript.

Preprint Disclosure Statement This manuscript was previously published as a pre-print on bioRxiv, available at https://doi.org/10.1101/2024.07.15.603535, on 17 July 2024.

References

Agnati LF, Guidolin D, Guescini M, Genedani S, Fuxe K (2010) Understanding wiring and volume transmission. Brain Res Rev 64(1):137–159. https://doi.org/10.1016/j.brainresrev.2010.03.003

Ahuja CS, Wilson JR, Nori S, Kotter MRN, Druschel C, Curt A, Fehlings MG (2017) Traumatic spinal cord injury. Nat Rev Dis Primers 27(3):17018. https://doi.org/10.1038/nrdp.2017.18

Allen AR (1911) Surgery of experimental lesion of spinal cord equivalent to crush injury of fracture dislocation of spinal column: a preliminary report. JAMA LVII(11):878. https://doi.org/10.1001/jama.1911.04260090100008

Aomura S, Nakadate H, Kaneko Y, Nishimura A, Willinger R (2016) Stretch-induced functional disorder of axonal transport in the cultured rat cortex neuron. Integr Mol Med 3:654–660. https://doi.org/10.15761/IMM.1000218

Apicella R, Taccola G (2023) Passive limb training modulates respiratory rhythmic bursts. Sci Rep 13(1):7226. https://doi.org/10.1038/s41598-023-34422-2

Basso DM, Beattie MS, Bresnahan JC, Anderson DK, Faden AI, Gruner JA, Holford TR, Hsu CY, Noble LJ, Nockels R, Perot PL, Salzman SK, Young W (1996) MASCIS evaluation of open field locomotor scores: effects of experience and teamwork on reliability. Multicenter Animal Spinal Cord Injury Study. J Neurotrauma 13(7):343–359. https://doi.org/10.1089/neu.1996.13.343

Bottlang M, Sommers MB, Lusardi TA, Miesch JJ, Simon RP, Xiong ZG (2007) Modeling neural injury in organotypic cultures by application of inertia-driven shear strain. J Neurotrauma 24(6):1068–1077. https://doi.org/10.1089/neu.2006.3772

Boulenguez P, Liabeuf S, Bos R, Bras H, Jean-Xavier C, Brocard C, Stil A, Darbon P, Cattaert D, Delpire E, Marsala M, Vinay L (2010) Down-regulation of the potassium-chloride cotransporter KCC2 contributes to spasticity after spinal cord injury. Nat Med 16(3):302–307. https://doi.org/10.1038/nm.2107

Carlson SL, Parrish ME, Springer JE, Doty K, Dossett L (1998) Acute inflammatory response in spinal cord following impact injury. Exp Neurol 151(1):77–88. https://doi.org/10.1006/exnr.1998.6785

Carreon LY, Glassman SD, Campbell MJ (2004) Pediatric spine fractures: a review of 137 hospital admissions. J Spinal Disord Tech 17(6):477–482. https://doi.org/10.1097/01.bsd.0000132290.50455.99

Cazalets JR (2005) Metachronal propagation of motoneurone burst activation in isolated spinal cord of newborn rat. J Physiol 568(Pt 2):583–597. https://doi.org/10.1113/jphysiol.2005.086850

Clarke EC, Cheng S, Bilston LE (2009) The mechanical properties of neonatal rat spinal cord in vitro, and comparisons with adult. J Biomech 42(10):1397–1402. https://doi.org/10.1016/j.jbiomech.2009.04.008

Danneman PJ, Mandrell TD (1997) Evaluation of five agents/methods for anesthesia of neonatal rats. Lab Anim Sci 47(4):386–395

Davis JA, Grau JW (2023) Protecting the injured central nervous system: do anesthesia or hypothermia ameliorate secondary injury? Exp Neurol 363:114349. https://doi.org/10.1016/j.expneurol.2023.114349

Del Negro CA, Funk GD, Feldman JL (2018) Breathing matters. Nat Rev Neurosci 19(6):351–367. https://doi.org/10.1038/s41583-018-0003-6

Ditunno JF, Little JW, Tessler A, Burns AS (2004) Spinal shock revisited: a four-phase model. Spinal Cord 42(7):383–395. https://doi.org/10.1038/sj.sc.3101603

Dose F, Deumens R, Forget P, Taccola G (2016) Staggered multi-site low-frequency electrostimulation effectively induces locomotor patterns in the isolated rat spinal cord. Spinal Cord 54(2):93–101. https://doi.org/10.1038/sc.2015.106

Eidelberg E, Sullivan J, Brigham A (1975) Immediate consequences of spinal cord injury: possible role of potassium in axonal conduction block. Surg Neurol 3(6):317–321

Eleraky MA, Theodore N, Adams M, Rekate HL, Sonntag VK (2000) Pediatric cervical spine injuries: report of 102 cases and review of the literature. J Neurosurg 92(1 Suppl):12–17. https://doi.org/10.3171/spi.2000.92.1.0012

Etlin A, Blivis D, Ben-Zwi M, Lev-Tov A (2010) Long and short multifunicular projections of sacral neurons are activated by sensory input to produce locomotor activity in the absence of supraspinal control. J Neurosci 30(31):10324–10336. https://doi.org/10.1523/JNEUROSCI.1208-10.2010

Gad P, Gerasimenko Y, Zdunowski S, Turner A, Sayenko D, Lu DC, Edgerton VR (2017) Weight bearing over-ground stepping in an exoskeleton with non-invasive spinal cord neuromodulation after motor complete paraplegia. Front Neurosci 8(11):333. https://doi.org/10.3389/fnins.2017.00333

Gao BX, Ziskind-Conhaim L (1995) Development of glycine- and GABA-gated currents in rat spinal motoneurons. J Neurophysiol 74(1):113–121. https://doi.org/10.1152/jn.1995.74.1.113

Geisler FH, Coleman WP, Grieco G, Poonian D, Sygen Study Group (2001) Measurements and recovery patterns in a multicenter study of acute spinal cord injury. Spine (Phila Pa 1976) 26(24 Suppl):S68-86. https://doi.org/10.1097/00007632-200112151-00014

Gerasimova E, Burkhanova G, Chernova K, Zakharov A, Enikeev D, Khaertdinov N, Giniatullin R, Sitdikova G (2021) Hyperhomocysteinemia increases susceptibility to cortical spreading depression associated with photophobia, mechanical allodynia, and anxiety in rats. Behav Brain Res 9(409):113324. https://doi.org/10.1016/j.bbr.2021.113324

Giraudin A, Cabirol-Pol MJ, Simmers J, Morin D (2008) Intercostal and abdominal respiratory motoneurons in the neonatal rat spinal cord: spatiotemporal organization and responses to limb afferent stimulation. J Neurophysiol 99(5):2626–2640. https://doi.org/10.1152/jn.01298.2007

Goodman RM, Wachs K, Keller S, Black P (1985) Spontaneous spinal cord "injury potential" in the rat. Neurosurgery 17(5):757–759. https://doi.org/10.1227/00006123-198511000-00005

Gorji A, Zahn PK, Pogatzki EM, Speckmann EJ (2004) Spinal and cortical spreading depression enhance spinal cord activity. Neurobiol Dis 15(1):70–79. https://doi.org/10.1016/j.nbd.2003.09.014

Guttmann L (1976) Spinal shock. Handbook of clinical neurology. North-Holland Publishing Co, Amsterdam

Hermann DM, Mies G, Hossmann KA (1999) Biochemical changes and gene expression following traumatic brain injury: Role of spreading depression. Restor Neurol Neurosci 14(2):103–108

Hiersemenzel LP, Curt A, Dietz V (2000) From spinal shock to spasticity: neuronal adaptations to a spinal cord injury. Neurology 54(8):1574–1582. https://doi.org/10.1212/WNL.54.8.1574

Hsu LJ, Bertho M, Kiehn O (2023) Deconstructing the modular organization and real-time dynamics of mammalian spinal locomotor networks. Nat Commun 14(1):873. https://doi.org/10.1038/s41467-023-36587-w

Iizuka M (1999) Intercostal expiratory activity in an in vitro brainstem–spinal cord–rib preparation from the neonatal rat. J Physiol 520(Pt 1):293–302. https://doi.org/10.1111/j.1469-7793.1999.00293.x

Janczewski WA, Onimaru H, Homma I, Feldman JL (2002) Opioid-resistant respiratory pathway from the preinspiratory neurones to abdominal muscles: in vivo and in vitro study in the newborn rat. J Physiol 545(3):1017–1026. https://doi.org/10.1113/jphysiol.2002.023408

Khristy W, Ali NJ, Bravo AB, de Leon R, Roy RR, Zhong H, London NJ, Edgerton VR, Tillakaratne NJ (2009) Changes in GABAA receptor subunit gamma 2 in extensor and flexor motoneurons and astrocytes after spinal cord transection and motor training. Brain Res 1273:9–17. https://doi.org/10.1016/j.brainres.2009.03.060

Kiehn O (2006) Locomotor circuits in the mammalian spinal cord. Annu Rev Neurosci 29:279–306. https://doi.org/10.1146/annurev.neuro.29.051605.112910

Kiehn O, Kjaerulff O (1996) Spatiotemporal characteristics of 5-HT and dopamine-induced rhythmic hindlimb activity in the in vitro neonatal rat. J Neurophysiol 75(4):1472–1482. https://doi.org/10.1152/jn.1996.75.4.1472

Kirshblum S, Snider B, Eren F, Guest J (2021) Characterizing natural recovery after traumatic spinal cord injury. J Neurotrauma 38(9):1267–1284. https://doi.org/10.1089/neu.2020.7473

Kitzman P (2005) Alteration in axial motoneuronal morphology in the spinal cord injured spastic rat. Exp Neurol 192(1):100–108. https://doi.org/10.1016/j.expneurol.2004.10.021

Kjaerulff O, Barajon I, Kiehn O (1994) Sulphorhodamine-labeled cells in the neonatal rat spinal cord following chemically induced locomotor activity in vitro. J Physiol 478(Pt 2):265–273. https://doi.org/10.1113/jphysiol.1994.sp020248

Kjell J, Olson L (2016) Rat models of spinal cord injury: from pathology to potential therapies. Dis Model Mech 9(10):1125–1137. https://doi.org/10.1242/dmm.025833

Kwo S, Young W, Decrescito V (1989) Spinal cord sodium, potassium, calcium, and water concentration changes in rats after graded contusion injury. J Neurotrauma 6(1):13–24. https://doi.org/10.1089/neu.1989.6.13

LaPlaca MC, Cullen DK, McLoughlin JJ, Cargill RS 2nd (2005) High rate shear strain of three-dimensional neural cell cultures: a new in vitro traumatic brain injury model. J Biomech 38(5):1093–1105. https://doi.org/10.1016/j.jbiomech.2004.05.032

Leao AA (1944) Spreading depression of activity in the cerebral cortex. J Neurophysiol 7(6):359–390. https://doi.org/10.1152/jn.1944.7.6.359

Leao AA (1947) Further observations on the spreading depression of activity in the cerebral cortex. J Neurophysiol 10(6):409–414. https://doi.org/10.1152/jn.1947.10.6.409

Li Y, Lucas-Osma AM, Black S, Bandet MV, Stephens MJ, Vavrek R, Sanelli L, Fenrich KK, Di Narzo AF, Dracheva S, Winship IR, Fouad K, Bennett DJ (2017) Pericytes impair capillary blood flow and motor function after chronic spinal cord injury. Nat Med 23(6):733–741. https://doi.org/10.1038/nm.4331

Liabeuf S, Stuhl-Gourmand L, Gackière F, Mancuso R, Sanchez Brualla I, Marino P, Brocard F, Vinay L (2017) Prochlorperazine increases KCC2 function and reduces spasticity after spinal cord injury. J Neurotrauma 34(24):3397–3406. https://doi.org/10.1089/neu.2017.5152

Lorach H, Galvez A, Spagnolo V, Martel F, Karakas S, Intering N, Vat M, Faivre O, Harte C, Komi S, Ravier J, Collin T, Coquoz L, Sakr I, Baaklini E, Hernandez-Charpak SD, Dumont G, Buschman R, Buse N, Denison T, van Nes I, Asboth L, Watrin A, Struber L, Sauter-Starace F, Langar L, Auboiroux V, Carda S, Chabardes S, Aksenova T, Demesmaeker R, Charvet G, Bloch J, Courtine G (2023) Walking naturally after spinal cord injury using a brain–spine interface. Nature 618(7963):126–133. https://doi.org/10.1038/s41586-023-06094-5

Lu Y, Zheng J, Xiong L, Zimmermann M, Yang J (2008) Spinal cord injury-induced attenuation of GABAergic inhibition in spinal dorsal horn circuits is associated with down-regulation of the chloride transporter KCC2 in rat. J Physiol 586(23):5701–5715. https://doi.org/10.1113/jphysiol.2008.152348

Malloy DC, Côté M-P (2024) Multi-session transcutaneous spinal cord stimulation prevents chloride homeostasis imbalance and the development of hyperreflexia after spinal cord injury in rat. Exp Neurol 376:114754. https://doi.org/10.1016/j.expneurol.2024.114754

Marcantoni M, Fuchs A, Löw P, Bartsch D, Kiehn O et al (2020) Early delivery and prolonged treatment with nimodipine prevents the development of spasticity after spinal cord injury in mice. Sci Transl Med 12(539):eaay0167. https://doi.org/10.1126/scitranslmed.aay0167

Marchetti C, Beato M, Nistri A (2001) Alternating rhythmic activity induced by dorsal root stimulation in the neonatal rat spinal cord in vitro. J Physiol 530(1):105–112. https://doi.org/10.1111/j.1469-7793.2001.0105m.x

Mazzone GL, Mohammadshirazi A, Aquino JB, Nistri A, Taccola G (2021) GABAergic mechanisms can redress the tilted balance between excitation and inhibition in damaged spinal networks. Mol Neurobiol 58(8):3769–3786. https://doi.org/10.1007/s12035-021-02370-5

Mekhael W, Begum S, Samaddar S, Hassan M, Toruno P et al (2019) Repeated anodal trans-spinal direct current stimulation results in long-term reduction of spasticity in mice with spinal cord injury. J Physiol 597(8):2201–2223. https://doi.org/10.1113/JP276952

Mladinic M, Nistri A, Taccola G (2013) Acute spinal cord injury in vitro: insight into basic mechanisms. In: Aldskogius H (ed) Animal models of spinal cord repair. Humana Press, Totowa, pp 39–62

Mohammadshirazi A, Apicella R, Zylberberg BA, Mazzone GL, Taccola G (2023) Suprapontine structures modulate brainstem and spinal networks. Cell Mol Neurobiol. https://doi.org/10.1007/s10571-023-01321-z

Nicholls JG, Stewart RR, Erulkar SD, Saunders NR (1990) Reflexes, fictive respiration and cell division in the brain and spinal cord of the newborn opossum, Monodelphis domestica, isolated and maintained in vitro. J Exp Biol. 152:1–15. https://doi.org/10.1242/jeb.152.1.1

Partida E, Mironets E, Hou S, Tom V (2016) Cardiovascular dysfunction following spinal cord injury. Neural Regen Res 11(2):189. https://doi.org/10.4103/1673-5374.177707

Robba C, Qeva E, Borsellino B, Aloisio S, Tosti G et al (2017) Effects of propofol or sevoflurane anesthesia induction on hemodynamics in patients undergoing fiberoptic intubation for cervical spine surgery: a randomized, controlled, clinical trial. J Anaesthesiol Clin Pharmacol 33(2):215. https://doi.org/10.4103/0970-9185.209733

Sadeghinezhad J, Nyengaard JR (2021) Morphometry of cervical spinal cord in cat using design-based stereology. Anat Histol Embryol 50(4):746–755. https://doi.org/10.1111/ahe.12719

Salzman SK, Lee WA, Sabato S, Mendez AA, Agresta CA et al (1993) Halothane anesthesia is neuroprotective in experimental spinal cord injury: early hemodynamic mechanisms of action. Res Commun Chem Pathol Pharmacol 80(1):59–81

Streit DS, Ferreira Filho CR, Martins-Ferreira H (1995) Spreading depression in isolated spinal cord. J Neurophysiol 74(2):888–890. https://doi.org/10.1152/jn.1995.74.2.888

Taber KH, Hurley RA (2014) Volume transmission in the brain: beyond the synapse. J Neuropsychiatry Clin Neurosci 26(1):iv–4. https://doi.org/10.1176/appi.neuropsych.13110351

Taccola G, Nistri A (2005) Characteristics of the electrical oscillations evoked by 4-aminopyridine on dorsal root fibers and their relation to fictive locomotor patterns in the rat spinal cord in vitro. Neuroscience 132(4):1187–1197. https://doi.org/10.1016/j.neuroscience.2005.02.012

Taccola G, Margaryan G, Mladinic M, Nistri A (2008) Kainate and metabolic perturbation mimicking spinal injury differentially contribute to early damage of locomotor networks in the in vitro neonatal rat spinal cord. Neuroscience 155(2):538–555. https://doi.org/10.1016/j.neuroscience.2008.06.008

Taccola G, Mladinic M, Nistri A (2010) Dynamics of early locomotor network dysfunction following a focal lesion in an in vitro model of spinal injury. Eur J Neurosci 31(1):60–78. https://doi.org/10.1111/j.1460-9568.2009.07040.x

Taccola G, Gad P, Culaclii S, Ichiyama RM, Liu W et al (2020) Using EMG to deliver lumbar dynamic electrical stimulation to facilitate cortico-spinal excitability. Brain Stimul 13(1):20–34. https://doi.org/10.1016/j.brs.2019.09.013

Takahashi T (1990) Inward rectification in neonatal rat spinal motoneurones. J Physiol 423(1):47–62. https://doi.org/10.1113/jphysiol.1990.sp018010

Wang MY, Hoh DJ, Leary SP, Griffith P, McComb JG (2004) High rates of neurological improvement following severe traumatic pediatric spinal cord injury. Spine 29(13):1493–1497. https://doi.org/10.1097/01.BRS.0000129026.03194.0F

Wang AH, Zhang GH, Zhang C, Huo XL, Song T (2015) Injury potentials of spinal cord in ex vivo compression injury model. IEEE 4659–4662.

Whelan P, Bonnot A, O'Donovan MJ (2000) Properties of rhythmic activity generated by the isolated spinal cord of the neonatal mouse. J Neurophysiol 84(6):2821–2833. https://doi.org/10.1152/jn.2000.84.6.2821

Williams AM, Manouchehri N, Erskine E, Tauh K, So K et al (2020) Cardio-centric hemodynamic management improves spinal cord oxygenation and mitigates hemorrhage in acute spinal cord injury. Nat Commun 11(1):5209. https://doi.org/10.1038/s41467-020-18905-8

Wilson RJA, Chersa T, Whelan PJ (2003) Tissue PO2 and the effects of hypoxia on the generation of locomotor-like activity in the in vitro spinal cord of the neonatal mouse. Neuroscience 117(1):183–196. https://doi.org/10.1016/S0306-4522(02)00831-X

Wrathall JR, Pettegrew RK, Harvey F (1985) Spinal cord contusion in the rat: production of graded, reproducible, injury groups. Exp Neurol 88(1):108–122. https://doi.org/10.1016/0014-4886(85)90117-7

Young W, Bracken MB (1992) The second national acute spinal cord injury study. J Neurotrauma 9(Suppl 1):S397-405

Young W, Koreh I (1986) Potassium and calcium changes in injured spinal cords. Brain Res 365(1):42–53. https://doi.org/10.1016/0006-8993(86)90720-1

Authors and Affiliations

Atiyeh Mohammadshirazi[1,2] · Graciela L. Mazzone[3,4] · Benjamín A. Zylberberg[3,4] · Giuliano Taccola[1,2]

✉ Giuliano Taccola
taccola@sissa.it

Atiyeh Mohammadshirazi
amohamma@sissa.it

Graciela L. Mazzone
gmazzone@austral.edu.ar

Benjamín A. Zylberberg
bzylberberg@austral.edu.ar

[1] Neuroscience Department, International School for Advanced Studies (SISSA), Via Bonomea 265, Trieste, TS, Italy

[2] Applied Neurophysiology and Neuropharmacology Lab, Istituto di Medicina Fisica e Riabilitazione (IMFR), Via Gervasutta 48, Udine, UD, Italy

[3] Instituto de Investigaciones en Medicina Traslacional (IIMT), CONICET-Universidad Austral, Av. Pte. Perón 1500, B1629AHJ Pilar, Buenos Aires, Argentina

[4] Facultad de Ciencias Biomédicas, Universidad Austral, Av. Pte. Perón 1500, B1629AHJ Pilar, Buenos Aires, Argentina